2010

Impact of Nickel Doping on Hydrogen Storage in Porous Metal-Organic Frameworks

Tanushree Banerjee
Virginia Commonwealth University

Impact of Nickel Doping on Hydrogen Storage in Porous Metal-Organic Frameworks

A thesis submitted in partial fulfillment of the requirement for
the degree of Master of Science in Chemistry at
Virginia Commonwealth University

by

TANUSHREE BANERJEE

B.Sc (Chemistry Hons), University of Burdwan, West Bengal, India
August, 1999

B.Ed (Education), Regional Institute of Education, Utkal University,
Orissa, India, July, 2002

Virginia Commonwealth University
Richmond, Virginia
August, 2010

Acknowledgement

I would like to express my gratitude to my advisor Dr. Hani El-Kaderi. I sincerely appreciate Dr. Puru Jena for his insightful advice, guidance and recommendations for my thesis. My sincere thanks to Dr. Vladimir Sidorov for his cooperation and constructive suggestion during the course of my graduate studies and my literature seminar. My thanks to Dr. James Terner for his suggestions made for my thesis. I thoroughly enjoyed taking the Chem 510 class with him while I was pregnant with my son. I would like to express my gratitude to Dr. Sarah Rutan, who has been a source of constant support, her graduate academic guidance and advice. I sincerely thank Dr. Sally Hunnicutt for the teaching assignments which gave me the confidence I needed to pursue my career goal. I thank my group members, especially Karl Jackson for helping me with the autosorb. I am grateful to Virginia Commonwealth University, Department of Chemistry for the financial support.

I thank my husband Dr. Nitai Mukhopadhyay and my son Moitreyo Mukhopadhyay for their immense love, support and understanding throughout my graduate school years. My Ma and Baba has been a constant source of inspiration. Last, but not least I thank my friend Daniel A Gerard for his support and guidance with software. He was always willing to help and share ideas and knowledge. I thank him for all his help.

Dedicated to my Baba and Ma

Table of Contents

Chapter 3:

List of Tables

List of Figures

Abbreviations and Symbols

ppm	Parts per million
wt%	weight percent
g/L	gram per litres
atm	atmosphere
°C	degree centigrade
K	Kelvin
Å	Angstrom
kg	kilogram
km	kilometer
MJ/m^3	Mega joule per cubic meter
kJ/g	kilo joule per gram
KJ/ mol	kilo joule per mole
kg H_2 /m^3	kilogram of hydrogen per cubic meter
cm^3/g	cubic centimeter per gram
MPa	Mega Pascal
keV	kilo electron volts
CO_2	Carbon dioxide
FCV	Fuel cell vehicle

SWCNT	Single walled carbon nanotubes
MWCNT	Multiwalled carbon nanotubes
DOE	Department of energy
MOF	Metal-organic framework
SBU	Secondary building units
MIL-101	Matériaux de l'Institut Lavoisier No.101
ST	Supertetrahedra
TEM	Transmission electron microscopy
XRD	X-ray diffraction
3c-2e	Three centered two electrons
NLDFT	Non-Local Density Functional Theory
GCMC	Grand Canonical Monte Carlo

Abstract

A supply of clean, carbon neutral and sustainable energy is the most scientific and technical challenge that humanity is facing in the 21st century. Though there is enough fossil fuels available for a few centuries, their use would increase the level of CO_2 in the atmosphere.[1] This would lead to global warming and may pose serious threats such as rising of sea level, change in hydrological cycle, etc. Hence there is a need for an alternative source of fuel that is clean and sustainable. Among the many resources considered as an alternative power source, hydrogen is considered one of the most promising candidates. To use hydrogen commercially, appropriate hydrogen storage system is required.

Various options to store hydrogen for onboard use include gaseous form in high-pressure tanks, liquid form in cryogenic conditions, solid form in chemical or metal hydrides, or by physisorption of hydrogen on porous materials.[2] One of the emerging porous materials are metal-organic frameworks (MOFs) which provide several advantages over zeolites and carbon materials because the MOFs can be designed to possess variable pore size, dimensions, and metrics.[3] In general, MOFs adsorb hydrogen through weak interactions such as London dispersion and electrostatic potential which lead to low binding enthalpies in the range of 4 to 10 kJ/mol. As a result, cryogenic conditions are required to store sufficient amounts of hydrogen inside MOFs. Up to date several MOFs have been designed and tested for hydrogen storage at variable temperature and pressure levels. The overall results thus far suggest that the use of

MOFs for hydrogen storage without chemical and electronic modifications such as doping with electropositive metals or incorporating low density elements such as boron in the MOFs backbone will not yield practical storage media. Such modifications are required to meet gravimetric and volumetric constraints. With these considerations in mind, we have selected a Cr-based MOF (MIL-101; $Cr(F,OH)\text{-}(H_2O)_2O[(O_2C)\text{-}C_6H_4\text{-}(CO_2)]_3 \cdot nH_2O$ ($n \approx 25$)) to investigate the impact of nickel inclusion inside the pores of MIL-101 on its performance in hydrogen storage. MIL-101 has a very high Langmuir surface area (5900 m^2/g) and two types of mesoporous cavities (2.7 and 3.4 nm) and exhibits exceptional chemical and thermal stabilities. Without any modifications, MIL-101 can store hydrogen reversibly with adsorption enthalpy of 10 kJ/mol which is the highest ever reported among MOFs. At 298 K and 86 bar, MIL-101 can store only 0.36 wt% of hydrogen.[4] Further improvement of hydrogen storage to 5.5 wt% at 40 bar was achieved only at low temperatures (77.3 K).[5] As reported in the literature, hydrogen storage could be improved by doping metals such as Pt. Doping is known to improve hydrogen storage by spillover mechanism [6 7] and Kubas[8] interaction. Hence we proposed that doping MIL-101 with a relatively light metal possessing large electron density could improve hydrogen adsorption. Preferential Ni doping of the MIL-101's large cavities which usually do not contribute to hydrogen uptake is believed to improve hydrogen uptake by increasing the potential surface in those cavities. We have used incipient wetness impregnation method to dope MIL-101 with Ni nanoparticles (NPs) and investigated their effect on hydrogen uptake at 77.3 K and 298 K, at 1 bar. In addition, the impact of metal doping on the surface area and pore size distribution of the parent MIL-101 was addressed. Metal content and NPs size was investigated by ICP and TEM, respectively. Furthermore, crystallinity of the resulting doped samples was confirmed by

Powder X-ray Diffraction (PXRD) technique. The results of our studies on the successful doping with Ni NPs and their impact on hydrogen adsorption are discussed.

Chapter 1

Introduction

All living things need energy to survive. The primary source of energy in the past was provided mainly from biomass, primarily wood. But after the industrial revolution, the increasing demand of energy was met from fossil fuel, mainly coal, for machines to work. In the past two centuries, the energy source has shifted from being dominated by coal to oil and natural gas. Currently the major fossil fuels that we are dependent on are petroleum, natural gas and coal. Fossil fuels primarily petroleum and recently natural gas are used in automobile industry. But consumption of these fossil fuels has serious consequences on the environment. Natural gas is widely used as a fuel. Our increasing demands for natural gas far exceed its current rate of production. It has been estimated that 60-160 years of natural gas reserves are available. However, burning of natural gas releases CO_2 into the atmosphere and it is considered to be a non-renewable source of energy. The petroleum reserve would last for another 50-150 years. But the use of oil and petroleum is increasing and projected to increase more as the population and the economy grow. Though the consumption is increasing, the production reached its peak during 1970's and is currently in a declining phase. Hence petroleum reserves would deplete soon. To meet the ever increasing need for oil, a large portion of it is imported from other countries which increases the cost and will make countries depend on other oil producing countries for fuel. In addition, burning of fossil fuel emits CO_2 into the atmosphere. The atmospheric CO_2 concentration has been between 210 and 300 ppm for the past 420,000 years.

But due to the CO_2 emission from the use of fossil fuel, the concentration of CO_2 in the past 50 years have been rising, and is now in excess of 380 ppm.[1] It has been projected to increase to 750 ppm by 2050. But the goal is to stabilize the atmospheric CO_2 to 550-650 ppm range. Even at the 550 ppm range issues such as rise in sea level, change in the hydrological cycle and other effects are predicted.[9] Hence there is an increased concern for a future fuel that would be environmentally benign.

1.1. Need for Alternative Source of Fuel

A supply of clean, carbon neutral and sustainable energy is the most scientific and technical challenge that humanity is facing in the 21st century. Non-renewable energy like petroleum would deplete soon if used at the current rate. In addition their use would increase the level of CO_2 in the atmosphere. Since carbon based fuels are becoming serious threats to the environment by increasing green house gas, there is need for alternative source of fuel that would have no or very few adverse environmental impacts. Nontraditional source made from biomass resource, for example ethanol, methanol, biodiesel and gaseous fuels such as hydrogen and methane are considered as alternative fuels for future.

1.1.1 Aspects of Hydrogen as an Alternative Fuel

Hydrogen is considered one of the most promising alternative sources of energy. The question that arises is how and why hydrogen is a desirable fuel. The first reason is its availability. Hydrogen is the third most abundant element on earth. It is mostly present in the form of water and hydrides and organic molecules. Hydrogen can be produced from biomass and natural gas which are basically hydrocarbon[10]. Hydrogen can be produced by splitting water, either by electrolysis or using sunlight as well as enzymes. The most successful method is using electrolysis. But if electricity used for electrolysis comes from fossil fuel, then it is again not

clean. It is, therefore, desirable that electricity used to split water comes from clean renewable energy sources. The sources for hydrogen are available in all countries. This would essentially allow us to achieve energy independence. The second reason is that it is a clean source of fuel. Combustion of hydrogen with oxygen produces pure steam which again has many applications in industrial processes and space heating. Due to absolutely no green house gas emission and direct combustion in engines with water as the only byproduct, hydrogen could be used for generating electricity from fuel cells to drive vehicles for future transportation. As water can be recycled back to produce hydrogen it can be sustainable, which is another desirable feature. Green house gas emission is highest for vehicles which run on gasoline. Hybrid electric vehicles which are currently available in the market have reduced the green house gas emission to a certain level. But if we start using hydrogen fuel cell vehicles we can significantly reduce the green house gas emission. This is evident from the fact that the car manufacturers are competitively experimenting to produce hydrogen based fuel cell cars.

1.2. Hydrogen Storage

Hydrogen is very high in energy content by weight (about 3 times more than gasoline), but has a very low energy content by volume (about 4 times less than gasoline).[11] This makes hydrogen storage a great challenge, particularly within the size and weight constraint of a vehicle. The target set by US department of energy for on board hydrogen storage by the year 2010 is 6.0 wt% (gravimetric) and 4.5 g/L (volumetric) at ambient temperature (from -40 to 85 °C) and 100 atm or less pressure.[12] By 2015 the capacity should to be increased to 9.0 wt% and 8.1 g/L. Thus to use hydrogen commercially, an appropriate hydrogen storage system is needed that would be able to charge and discharge huge amounts of hydrogen at a rapid rate under ambient conditions with the above mentioned capacity, to meet commercial requirements. The

modern cars with combustion engine which are available in the market burn about 24 kg of petrol to run for 400 km. However, 8 kg of hydrogen needed for combustion engine version and only 4 kg hydrogen for electric car with fuel cell to cover the same range.[2] Unfortunately, hydrogen is very difficult to compress for on-board storage. For example, in gas phase 4 kg of hydrogen occupies 45 m^3 at room temperature and atmospheric pressure.[2]

1.3. Hydrogen Storage Methods

In this section, we summarize the various ways of storing hydrogen and recent developments in this field.

1.3.1. Conventional Hydrogen Storage Methods

1.3.1.1. ***Compressed Gas*.** Hydrogen is stored in high pressure tanks in the form of compressed gas. This way of transporting hydrogen is not safe. It is also not cost effective. Also compressed hydrogen gas tanks are large and heavy. The main disadvantages associated with gaseous hydrogen are low density and large storage volume as opposed to liquid hydrogen. A very high pressure is required to store hydrogen at room temperature (300-700 bar).[11].

1.3.1.2. ***Cryogenic Liquid.*** Liquefied hydrogen is denser and has higher energy content than the gaseous hydrogen at a given volume. Liquid hydrogen tanks store more hydrogen than the compressed gas tanks, but it takes energy to liquefy hydrogen and tank insulation is required. It is difficult to keep hydrogen in the liquid form because of the low liquid-gas phase change enthalpy of 0.45 kJ/g hydrogen.[5] Conventionally hydrogen is liquefied at high pressure and stored in tanks. In most countries high pressure tanks are made from inexpensive steel and can take up a pressure of up to 200 bar. These high pressure containers have major limitations, the fuel would be available only when the pressure is

dropped from 450 bar to zero overpressure, and hence additional pressure control is needed. The critical temperature of hydrogen is -241 °C, hence to prevent overpressure the liquid hydrogen containers are open systems.[2] So there is always loss of hydrogen. In addition, long distance transportation of hydrogen is only done as cryogenic liquid. But the problem is to maintain the low temperature (-253 °C) while transporting.[11] It is a technical challenge to manufacture a suitable cylinder which can maintain cryogenic temperature in order to store hydrogen for onboard storage.

Hence the conventional types of storage are not preferred due to their inherent drawbacks; other option is storing hydrogen chemically in the form of hydrides.

1.3.2. Chemical Hydrogen Storage Methods.

One of the methods to store hydrogen is to break dihydrogen molecules into hydrogen atoms and then incorporate them into solid lattice framework by surface adsorption. At low pressure and at ambient temperature, it is possible to store large amounts of hydrogen in a small volume. Typical materials are various hydrides like intermetallic, complex or chemical hydrides. Metal hydrides store hydrogen in a discrete M-H bond. Metal hydrides have high heat of enthalpies in the range of 80 KJ/mol. Hence energy is required to drive off hydrogen for use while huge amount of energy is released on recharging.[13]

1.3.2.1. ***Intermetallic Hydrides.*** Hydrogen can be reversibly stored in alloys in the form of intermetallic hydride ($LaNi_5H_{6.5}$). The advantage is that adsorption and desorption of hydrogen can be done at moderate pressures unlike elemental hydrides which need higher temperature and lower pressures for desorption. The alloys resulting from $LaNi_5$ shows fast and reversible sorption, however its use for hydrogen fuel tanks is not appropriate due to low H_2 weight percentage. Some intermetallic compounds form hydrides that contain up

to 9 mass% hydrogen. However hydrogen release from these hydrides is not reversible within the desired temperature and pressure ranges.[2]

1.3.2.2. ***Complex Hydrides.*** Generally, these are main group metal hydrides such as $LiAlH_4$. It is a complex formed from negatively charged metal hydride balanced by alkali metals Li, Na, etc. The main advantage of complex hydrides is that they can store higher hydrogen wt%, but their poor reversibility limits their use and make them undesirable.[13]

1.3.2.3. ***Chemical Hydrides:*** Hydrogen can also be stored in form of organic hydrides. For example, decalin is formed by heating naphthalene and hydrogen at 200 ^{o}C. Since covalent bonds are formed between hydrogen and the metal, low temperature is required for adsorption. Desorption requires higher temperature, which is not desirable for on-board storage. The problem associated with chemical hydrides is irreversible storage of hydrogen which requires heating and cooling for hydrogen discharging and charging respectively.[11, 2]

1.3.3. Physical Hydrogen Storage Methods

During physical storage, molecular hydrogen gets adsorbed through relatively weak interaction. When the interaction is governed by weak van der Waals force (dispersion interaction), then physical adsorption (physisorption) of molecular hydrogen on high surface area porous materials takes place.[14] Hydrogen gets adsorbed into high surface area porous materials and are dependent on the temperature and pressure.

1.4. Hydrogen Storage in Porous Materials

Porous materials are broadly divided into three categories depending on their size of the pores, (1) Microporous (diameter of the pore less than 2 nm/ 20Å), (2) Mesoporous (2-50 nm/ 20-500Å) (3) Macroporous (more than 50 nm/ 500Å).

Porous materials such as zeolites, MOF,[15] [16] carbon materials (carbon nanotubes,[17] activated carbon,[18] nanostructured carbon, carbon nanofibres,[18] mesocarbon microbead,[19] carbon aerogels,[20] ordered mesoporous carbon,[21] carbon monoliths),[22] are capable of storing hydrogen at low temperatures with variable performance. Physisorption of hydrogen by these high surface area materials needs cryogenic conditions. Porous materials are capable of storing physisorbed molecular hydrogen reversibly with fast kinetics as opposed to chemical adsorption. However physical adsorption of hydrogen is associated with issues like low adsorption enthalpy that result in low storage capacity at ambient conditions.

1.4.1. Hydrogen Storage in Zeolites and Molecular Sieves

Hydrogen could be stored in zeolite and molecular sieves by adsorption into the hollow space of the host molecule. It was found that the sodalite cages are the host where hydrogen is adsorbed. This is due to the fact that the kinetic diameter of hydrogen molecule is 0.29 Å and overlapping potential is possible only in sodalite cages. Also hydrogen can be stored in zeolites that only have sadalite cages. It is not conceivable to entrap hydrogen in the α-cages. It is possible to reversibly adsorp and desorp hydrogen; however the storage capacity is 9.2 cm^3/g at 573 K and 10.0 MPa which is much less than metal hydride storage systems which are about 150 to 700 cm^3/g.[23]

1.4.2. Hydrogen Storage in Carbon Nanotubes

Carbon nanofibers, single walled carbon nanotubes (SWCNT) and multiwalled carbon nanotubes (MWCNT) shows promising potential to store hydrogen. This is due to the electronic nature resulting from sp^2 hybridization, large surface area and molecular sized pores present in these carbon based materials. At moderate temperature and pressure, SWCNT show potential for

hydrogen storage. Results from literature shows MWCNT could store hydrogen from 1.975 at 40 bars to 6.3 wt% at 148 bar.[17a]

1.4.3. Metal-Organic Frameworks

MOFs are one, two or three dimensionally linked networks consisting of nodes, which are metal cations or di- tri- or tetra- or polynuclear metal cation cluster, connected to organic ligands commonly, di- tri- or tetradentate ligands. The organic linkers are primarily covalent while the inorganic part is ionocovalent (i.e. the bond involves electrostatic force (ionic part) and covalent forces resulting from the combination of atomic orbital of cations and anions). The coordination bonds between metals and ligands are strong and this gives rise to crystallographically well-defined open structure which is stable upon removal of guest molecules giving permanent porosity. A major feature of MOFs over zeolites and CNTs is that it can be designed[3] and then synthesized which is made possible by the concept of reticular synthesis.

1.4.3.1. Reticular synthesis

Building extended structures from metal ions and organic linkers is not efficient because simple metal ions possess little directional information. This deficiency in directional information causes flexibility around metal ion and diversity of possible structure and lack of control. In addition starting entities lose their structure during the course of reaction, which leads to poor correlation between reactant and product. These issues are addressed in "reticular chemistry", the new emerging field of science where molecular building units, also known as secondary building units (SBU), are stitched into extended structure through strong bonds to form crystalline solid state materials with fixed topology.[3] In reticular synthesis, the use of specific reaction conditions leads to in-situ formation of rigid and well-defined molecular building blocks that maintain their structural aspect and rigidity throughout the synthesis. Hence utilizing reticular synthesis, wide

range of MOF's are constructed from polyatomic inorganic metal cluster, usually first row transition metal (inorganic SBU) linked by polytopic chelating linkers (the organic SBU). Both the inorganic and organic SBUs can be of a variety of geometry ranging from linear to polygonal structures. In figure 1, geometries of some inorganic SBUs and organic SBUs are shown. Inorganic SBUs figure 1 (a, b, c and d) can be triangular, square, octahedral and prismatic and organic SBUs figure 1 (e, f and g) can be triangular, tetrahedral and square planar.[24] The metal ions are chelated by the carboxylate functionality of organic linker and lock them into rigid structure. These metal-oxygen-carbon clusters provide direction and point of extension. The carbon atoms in the cluster define the geometric shapes of the SBU. SBUs provide directionality for construction of MOF and also impart framework robustness. Thus the concept of SBU is advantageous in rationalizing the topologies of MOF structure. By utilizing structurally diverse inorganic and organic SBUs, large number of geometric structures can be synthesized. Formation of the predesigned network is a possibility if the reaction conditions are properly identified to produce an SBU in-situ with particular geometry. Thus, reticular chemistry involves designing, synthesizing and characterization of the structure in a predictable fashion.

This type of crystal chemistry offers MOF immense possibility to design structure and properties to a greater extent than that of zeolite where the main building block is the silicate tetrahedron rather than the SBU.[24] In MOFs the different functionalized organic linkers are directly added as reactant into the syntheses and the metal based units assemble in-situ during crystallization. Hence it is possible to generate series of compounds with same topology but different composition and dimension, both in principle and in practice by using organic linkers with same geometric arrangements of bonding group (commonly carboxylates and amines) but different organic molecules.

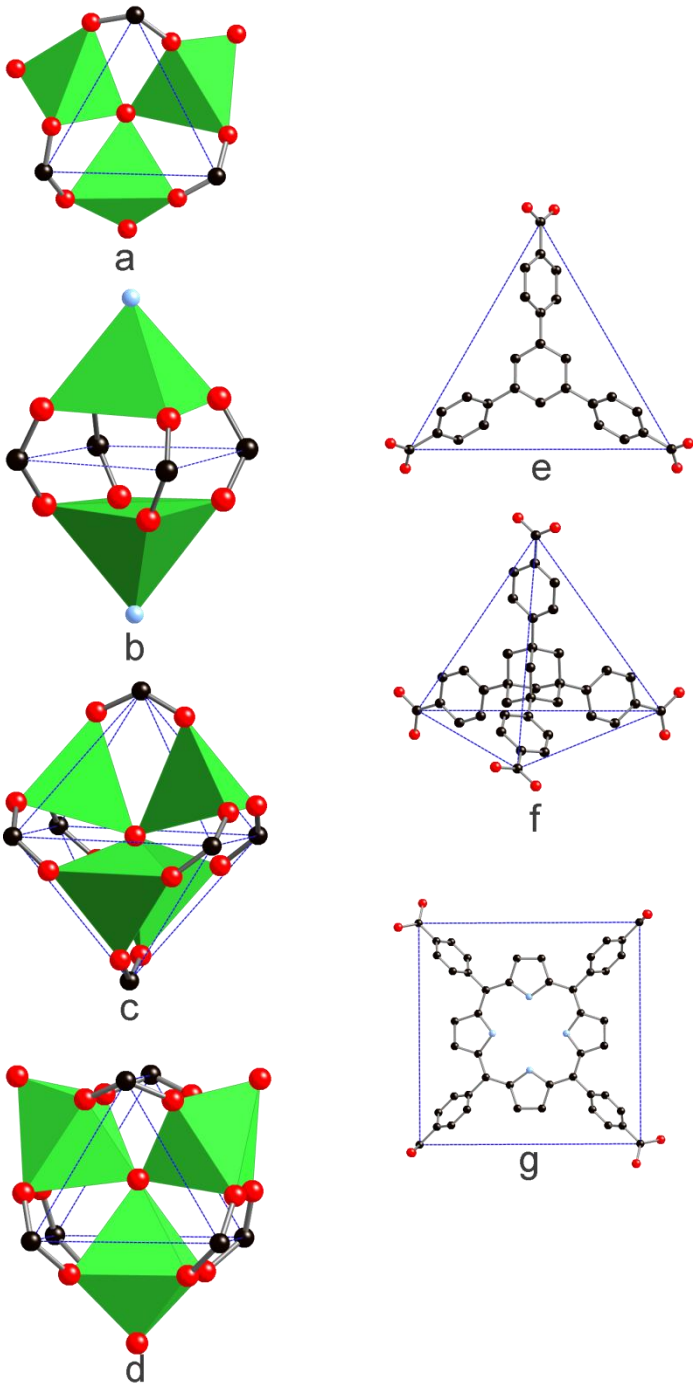

Figure 1: Inorganic SBUs (a, b, c, d) a: trigonal planar, b: square paddle-wheel, c: octahedral and d: trigonal prism. Organic SBUs (e, f, g) e: trigonal planar, f: tetrahedral and g: square planar. Blue dotted lines depict the geometry.

If inorganic moiety and organic linkers are chosen carefully, formation of desired kinds of pores are possible. Moreover the capability to modify the organic linker chemically, by organic synthesis, allows foreseeable synthesis of functionalized MOFs. The tunability and predictable design of MOF increases its usability in various applications. For the past 15 years, hybrid organic-inorganic mesoporous solids have gained significant importance for wide range of structures and properties such as their notable adsorption properties, high surface area, large pores size, and flexibility in structure, thermal stability, uncoordinated metal adsorption sites, high crystallinity and functionality of the framework, permanent porosity, dynamic porous properties, functionality of metal ion and organic ligands besides their key characteristic such as structural flexibility, design ability and regularity. In addition MOF are amazingly light and porous such that the surface area of one gram could cover an entire football ground. MOFs possess novel chemical, physical, electronic and magnetic properties. These properties allow wide range of applications in diverse fields such as optics, catalysis, ion exchange, gas storage, gas separation, sensing, polymerization and drug delivery, molecular electronics etc.

1.5. Advantages of MOFs over Related Zeolites and Carbon nanotubes (CNT)

Porous material like zeolite,[23] activated carbon,[25 26 27] and carbon nanotubes[17a] are used for gas storage purposes. However, MOF provides advantages over these materials because the size- and shape of pores inside MOFs are tunable.[28] So far MOFs are the one of best materials used for physical hydrogen storage. Porous MOFs permits guest molecules to penetrate through the pores without destroying the framework. Also the weakly coordinated species i.e. the guest water molecules are easily removed thermally or chemically and unsaturated metal sites are formed, which can further increase the adsorption of hydrogen. Hence metal-organic frameworks (MOF) are potential candidates to store substantial amounts of hydrogen at cryogenic conditions

(low temperature) and high pressure. Due to the small kinetic diameter (2.89 Å) of hydrogen molecules it interacts only with high potential surfaces. MOFs adsorb hydrogen through weak interactions such as London dispersion and electrostatic potential. Due to the low binding enthalpy 4-10 kJ/mol, resulting from such interactions, cryogenic conditions are preferred. The polarizability of the MOF material determines the dispersion interactions and the distance between the H_2 and potential surface. Hence, there is a preferential adsorption of hydrogen on the MOF within the pores in which the overlapped potential fields from both sides of pores strengthen the potential interaction. So increasing the following aspects would lead to enhanced hydrogen adsorption in MOFs: (i) High potential surface, (ii) Exposed metal sites,[29] [30] (iii) Binding enthalpy (20-30 kJ/mol).

1.6. Improved H_2 Storage in Zeolite and CNT by Doping with Transition Metals

In gas phase, chemical adsorption i.e. chemisorption of atomic hydrogen on CNT is not possible because dissociation energy of 440 kJ/mol is required to break the molecular H-H bond. However, transition metals for example Ni, Co, Pt has been found to act as active dissociative catalysts for hydrogen.[31] [32] It has been found in several studies, how metal doped porous materials have increased hydrogen uptake. In one such study Ni doped on MWCNT was investigated. Different loadings of 3, 6, 13, 40 wt% Ni nanoparticles dispersed on MWCNT was studied. In the gas phase Ni can dissociate hydrogen molecule and the atomic hydrogen thus formed interacts with surface of MWCNT through chemical bonds. This was confirmed by the fact that desorption activation energy was higher which means that the mechanism by which hydrogen gets stored is associated with some chemical interaction between hydrogen and carbon. In this study it was found that hydrogen uptake were 1.2, 2.8, 1.8, 0.4 wt% respectively at moderate temperature and pressure for 3, 6, 13, 40 wt% metal loading. The 6 wt% Ni loaded

MWCNT showed highest hydrogen uptake than the MWCNT without good Ni dispersion. It was also found that as more Ni distribution on MWCNT increased, proportionately the desorption temperature also increased. TEM images for the 6 wt% Ni shows that the Ni nanoparticles were ~1.2nm and were well distributed over MWCNT and showed maximum uptake. On the other hand, for higher Ni loading concentration of 40 and 13 wt%, TEM showed that the Ni nanoparticles aggregated and were about 10nm in size. For 3 wt% loading the Ni nanoparticles formed islands on the surface and does not show improvement in uptake.[33] These suggest that Ni nanoparticle plays a significant role in hydrogen adsorption on CNT surface and also dissociation of the hydrogen molecule.

1.7. Different Doping Methods

There are various methods of preparations of metal nanoparticles. The following table summarizes all different routes.[34]

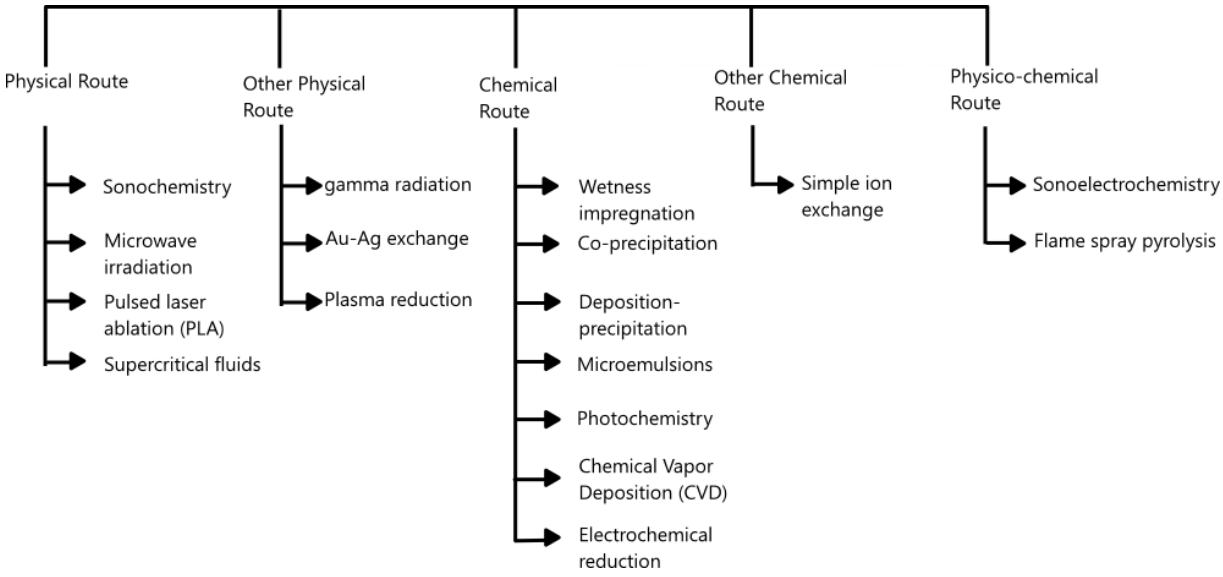

Table 1.1 Different doping methods for porous materials

1.8. Mechanisms by which Doping Improves Hydrogen Storage

1.8.1. Kubas Interaction

Nano sized metal clusters can interact with H_2 to form 3c-2e bonds through what is called Kubas interaction.[8] [35] In this kind of interaction, the bonding orbital of H_2 interact with the antibonding orbital of the metal. If the interaction is weak H_2 is just adsorbed to the d-orbitals of transition metals. If this interaction is strong the bond holding the H atoms break and atomic hydrogen forms. This exactly is what happens in spillover mechanism.

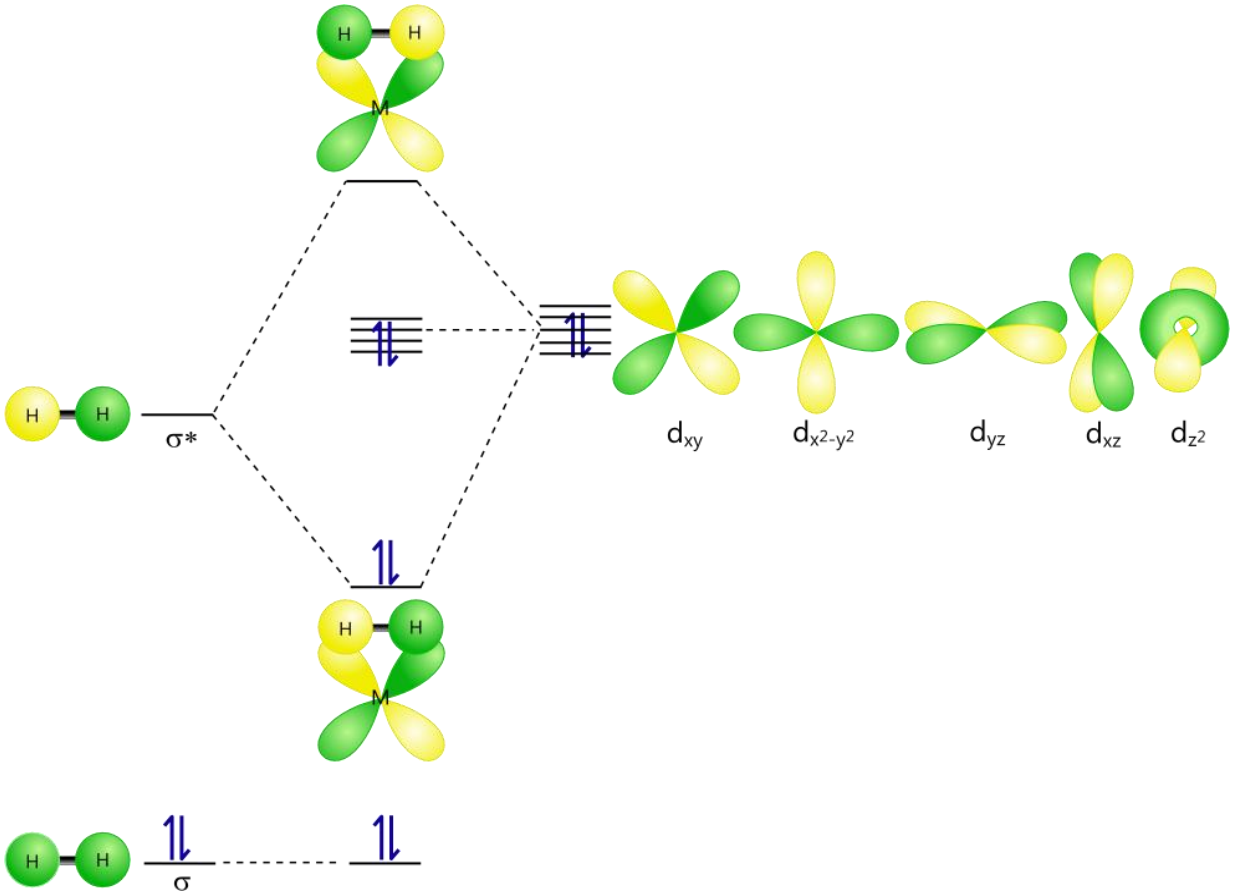

Figure 2. Interaction diagram of hydrogen molecule and metal d-orbital (Kubas interaction)

1.8.2. Spillover Mechanism

Hydrogen spillover is dissociative chemisorptions of hydrogen on the metal and subsequent migration of atomic hydrogen onto the surface of support. The support is the primary receptor for atomic H_2.[36 37 7]

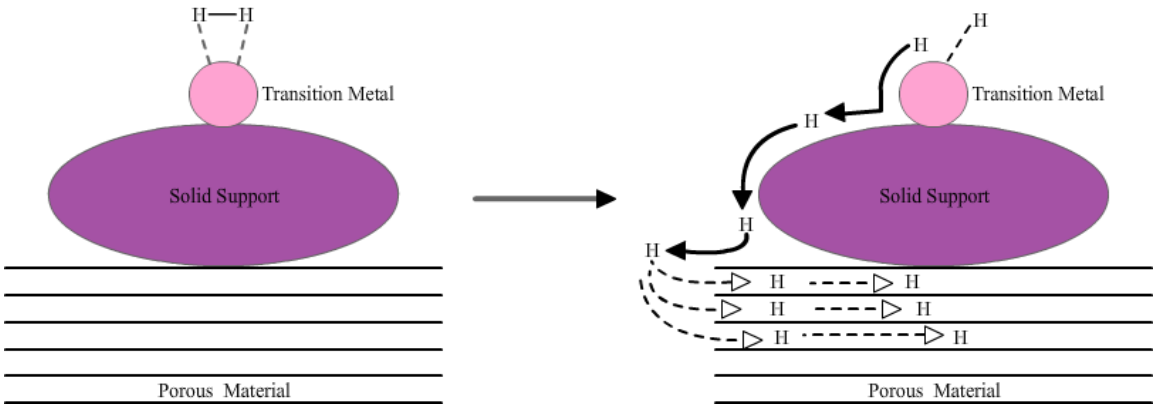

Figure 3. Hydrogen Spillover by metal nanoparticles

1.8.3. Charge Polarization Mechanism

Hydrogen interacts with the neutral atom through Kubas interactions or Spillover mechanism. However, hydrogen interacts with metal ion in a completely different fashion. When hydrogen molecule comes near transition metal ion, the metal ion is energetically incompetent to transfer electron to the hydrogen molecule. This is due to the fact that removing electrons from positive ion is not easy, because the second ionization potential of the transition metal atom is much higher than the first. Alternatively the metal ion polarizes the nearby hydrogen molecule by charge polarization mechanism. By dipole mechanism, bonding between metal ion and the hydrogen molecule takes place through simple electrostatic interaction. Hence, through charge polarization mechanism transition metal ions are capable of binding large number of molecular hydrogen and increase hydrogen uptake. It has been shown in literature that one Ni^+ ion could

trap about ten hydrogen molecules. That is hydrogen is "chemisorbed" on the Ni^+ ions in its molecular form. [38]

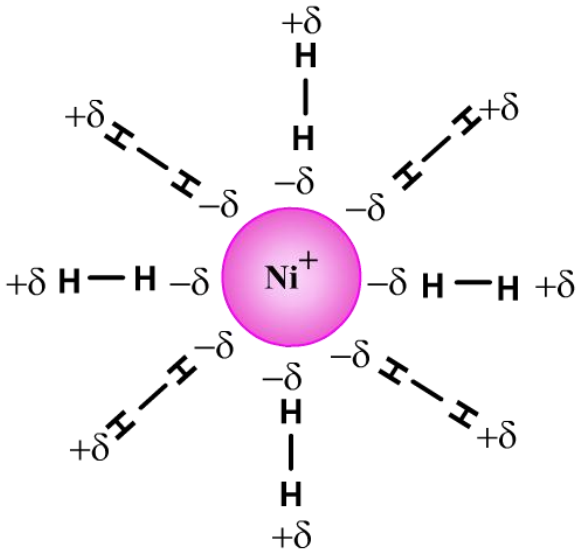

Figure 4. Charge polarization of hydrogen molecule by metal ion

The binding energy and geometry of hydrogen molecule interacting with Ni^+ ions have been studied in the literature. The Ni^+ ion has open electronic shells while hydrogen molecule has closed electronic shell but with high polarizability. Using Atkins model it is possible to determine the number of hydrogen molecules or atoms that could bind to a metal cation. [39]

It has been found in literature that the size of the metal cluster ion also plays an important role in hydrogen absorption. It has been found that small cluster with large ionization potential favors molecular bonding. It is energetically not favorable to donate electron to the anti-bonding orbital of H_2. Hence, the binding is associative. On the other hand large clusters with low ionization potential could prefer to donate electron to the anti-bonding orbital of H_2 and favor atomic bonding i.e. dissociative binding. [40] [41]

1.9. Different Methods of Preparation of MOF

Solvothermal Syntheses. Solvothermal syntheses are carried out above temperature of 100 ºC. The important factors *are* acidic pH, temperature and concentration. The most essential is the temperature. Normally water is used as the main solvent, but alcohols, dialkyl formamides, pyridines are also used.

Hydrothermal Synthesis. The dielectric properties of the solvent changes during hydrothermal conditions and that lead to weak interaction between solvent molecules and hence dissociation of the solvent molecules. For hydrothermal synthesis a mixture of non miscible solvents (for example heavy alcohol and water) are used. At the interface of biphasic mixture, the solid forms and most of the time gives a single crystal of the preferred phase.

Electrochemical Route. In electrochemical cells, bulk copper plates (thickness 5mm) are arranged at the anode with a copper cathode and carboxylates linker dissolved in methanol is used as the solvent. For a certain period of time, a voltage of 12-19V and a current of 1.3 A is applied. The product precipitates, which is then filtered and dried.[42]

Microwave Synthesis. Microwave method is used for synthesis of nanoporous inorganic material, which usually takes several days for hydrothermal crystallization. Microwave synthesis takes short crystallization time, produces narrow particle size distribution, and enables effective evaluation of process parameter and easy morphological control. MOF samples synthesized under microwave are purer in phase and have higher crystallinity.[43 44]

High Throughput Synthesis. High throughput (HT) method involves four main steps: design of the experiment, synthesis, characterization and data evaluation which needs to be incorporated in a workflow to attain a maximum productivity and innovation. In short time, HT method produce incredible amount of data.[45]

1.10. Thesis Problem

In spite of the many attractive features of MOFs such as their exceptionally high surface area, low density, and thermal stability which are relevant to hydrogen storage, their performance in hydrogen storage under desirable conditions remains modest as a result of their neutral surface which interacts weakly with hydrogen. For practical applications, post synthesis modification of MOFs by doping them with late transition metal NPs could lead to enhanced performance as a result of spillover or Kubas interactions. The work described in the following sections addresses the impact of Ni NPs doping of MIL-101 ($Cr_3F(H_2O)_2O[(O_2C)\text{-}C_6H_4\text{-}(CO_2)]_3.nH_2O$ where n is ~ 25) on its performance in hydrogen storage.

Chapter 2

Results and Discussion

2.1. Synthetic Aspect of MIL-101

Synthesis of MIL-101

MIL-101 was synthesized using methods described by Férey and co-workers[4] from hydrothermal reaction of terephthalic acid (166 mg, 1 mmol) with $Cr(NO_3)_3.9H_2O$ (400 mg, 1 mmol), fluorohydric acid (0.2 mL, 5.0 M), and H_2O (4.80 mL, 265 mmol).[4] The resultant mixture was introduced in a hydrothermal vessel and heated for 8 hours at 220 °C (equation 1). HF acts as mineralizing agent and increases the crystallinity of MIL-101.

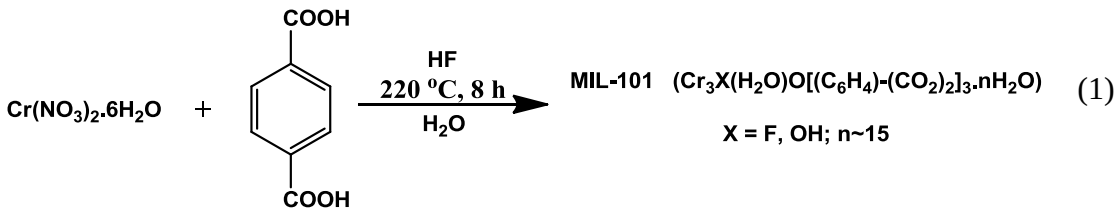

(1)

A substantial amount of recrystallized terephthalic acid is usually present after cooling to room temperature. To get rid of most of the recrystallized terephthalic acid, the mixture is filtered through coarse glass fritt filter, the water and the MIL-101 powder passes through the filter while the free acid stays inside the glass filter. After that fine fritt filter is used to separate MIL-101 powder from the suspension. A considerable amount of unreacted terephthalic acid exists both outside and within the pores of MIL-101. To eliminate the unreacted terephthalic acid the as-synthesized MIL-101 are activated using ethanol. A solvothermal treatment using 60 mL ethanol

(95% ethanol with 5% water) and 300 mg of as-synthesized MIL-101 was performed by introduced this mixture in a hydrothermal bomb for 20 hours at 100 °C. The resulting mixture is cooled and filtered through medium (M) fritt filter and washed with ethanol. Finally the solid is dried overnight at 150 °C. Based on elemental analysis this reaction produced crystallized green powder of chromium terephthalate: $Cr_3F(H_2O)_2O[(O_2C)\text{-}C_6H_4\text{-}(CO_2)]_3.nH_2O$ where n is ~ 25.

2.2. Structural Aspect of MIL-101

MIL-101 is a hybrid inorganic-organic solid which is constructed form organic moiety (1, 4-benzene dicarboxylic acid; BDC) anion and a pseudo-octahedral or prismatic inorganic SBU which is the trimeric chromium cluster as illustrated in Figure 5.

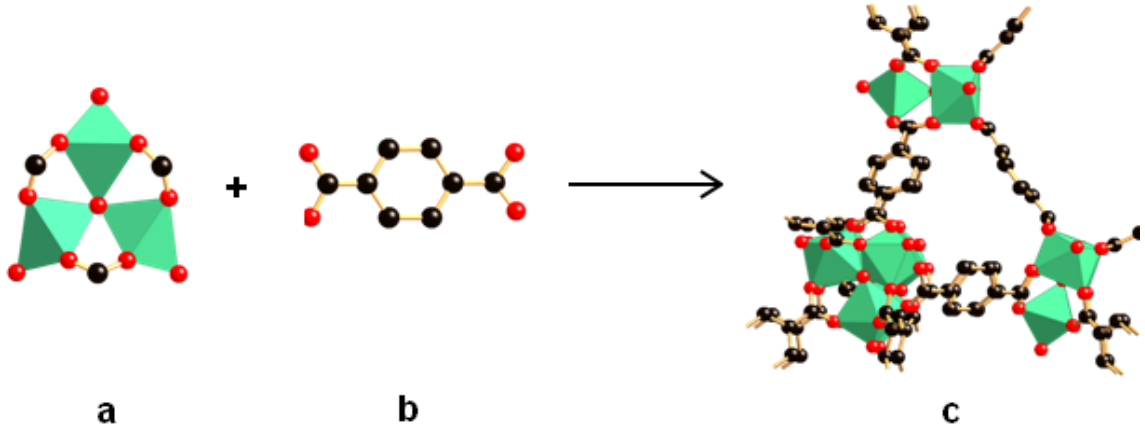

Figure 5. Structure of inorganic secondary unit (a), organic linker (b) and the resulting supertetrahedra (c).

The inorganic SBU ($Cr_3(\mu_3O)$ trimers) is formed by trivalent metal cations Cr^{3+} in an octahedral environment . The vertices of the pseudo-octahedral structure are occupied by the μ_3-O atoms in the middle of the chromium trimers and four oxygen atoms derived from the carboxylate group of the terephthalate linkers. The empty coordination sphere around chromium is completed by a water molecule, a fluorine atom or a hydroxyl group.[46] A microporous supertetrahedra (ST) is formed by the μ_3-oxo bridged trimeric chromium (III) octahedral cluster cross linked by

terephthalate ligand. In the ST, the four vertices are occupied by $Cr_3(\mu_3\text{-}O)$ trimers, and the organic linkers are located at the six edges of the ST. The connection between the ST is established through vertices to produce a 3D network of corner sharing superterahedra. These links are analogous to the way tetrahedrons are joined in the tetrahedrally linked MTN zeolite topology, but with larger unit cells.[46]

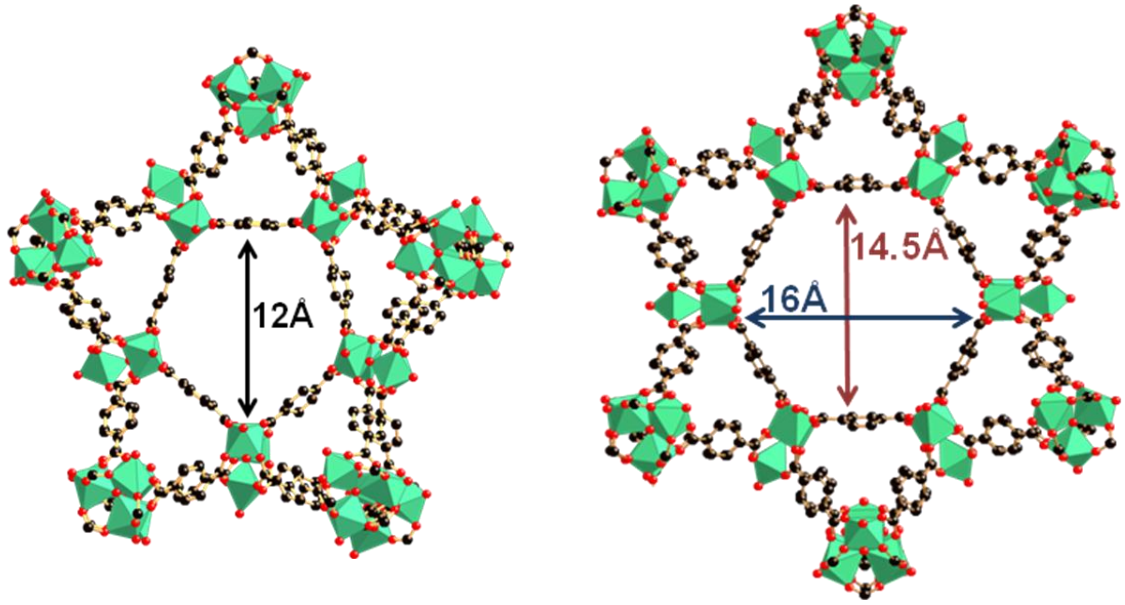

Figure 6. Structure of pentagonal window of size 12 Å (left) and hexagonal window of size 14.5 Å by 16 Å (right) present in MIL-101.

The ST is microporous with ~ 8.6 Å free apertures for the windows. MIL-101 has mesoporous cages, and microporous windows. There are two types of windows, one pentagonal and another hexagonal in shape (Figure 6). The very huge cell volume (~ 702,000 $Å^{3)}$ of MIL-101 results from two quasi- spherical cages (Figure 7). A smaller cage formed from 12 pentagonal faces/windows with free opening of ~12 Å and a larger cage formed by 12 pentagonal and 4 hexagonal faces/windows with ~ 14.5 Å by 16 Å free apertures. The two mesoporous cages are in 2:1 ratio and delimited by 20 and 28 ST with internal free diameter 29 Å and 34 Å,

respectively. Thus they contribute to the huge BET surface area 4100 ± 200 m^2/g and Langmuir surface 5900 ± 300 m^2/g of MIL-101.[47 4]

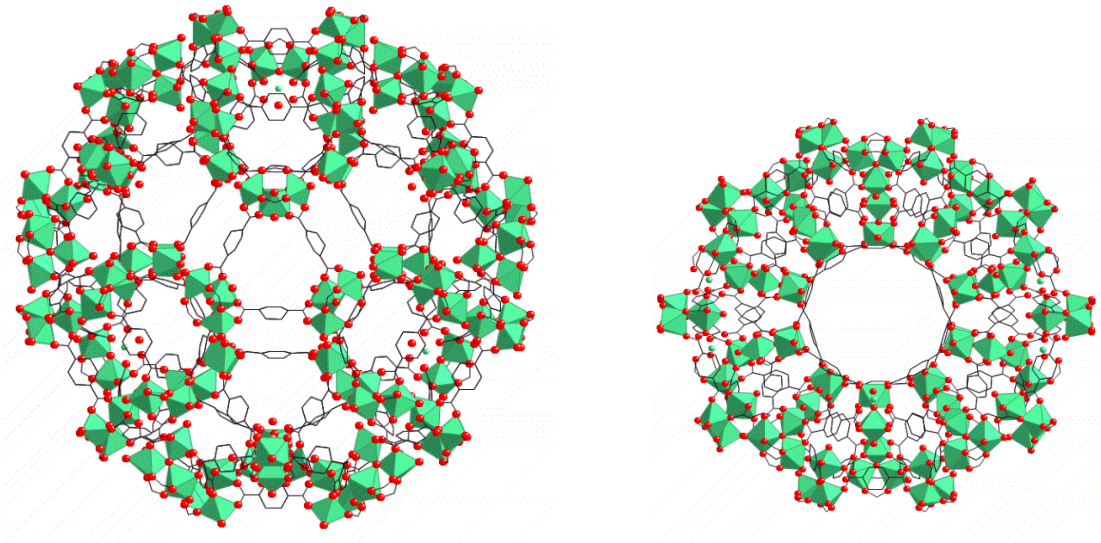

Figure 7. Structure of the cages. (Left) larger cage containing both pentagonal and hexagonal windows and (right) smaller cage containing only pentagonal windows.

2.3. Characteristic Features of MIL-101

MIL-101 has numerous extraordinary features such as mesoporous zeotype architecture with mesoporous cages and micro porous windows, high surface area, giant cell volume, and several unsaturated chromium sites. In MIL-101, the presence of unsaturated Cr (III) sites with electron rich functional group provides inherent chelating properties. Hence these aspects provide an effective way to selectively functionalize the unsaturated site in the MIL-101. Unsaturated Cr (III) sites,[30] which are hard Lewis acids could be used for immobilization and encapsulation of metal components, organic molecules etc. The thermal stability of MIL-101 is also high. MIL-101 decomposes above 300 $^{\circ}C$. These features make MIL-101 useful for adsorption/storage,[48] catalysis,[49 50 51 52 53] molecular recognition, novel co-ordination structure, gas separation,[54] drug delivery, luminescence, magnetism, conductivity, etc.

2.4. Characterization of MIL-101

2.4.1. X-Ray Diffraction (XRD)

The X-ray diffraction patterns were obtained from X'Pert Philips Diffractometer, with $CuK_{\alpha}R$ radiations. The XRD patterns for the experimental and theoretical MIL-101 are shown in Figure 8. XRD pattern from Figure 8 shows that the synthesized MIL-101 is coherent with the calculated one, implying that the MIL-101 made is authentic.

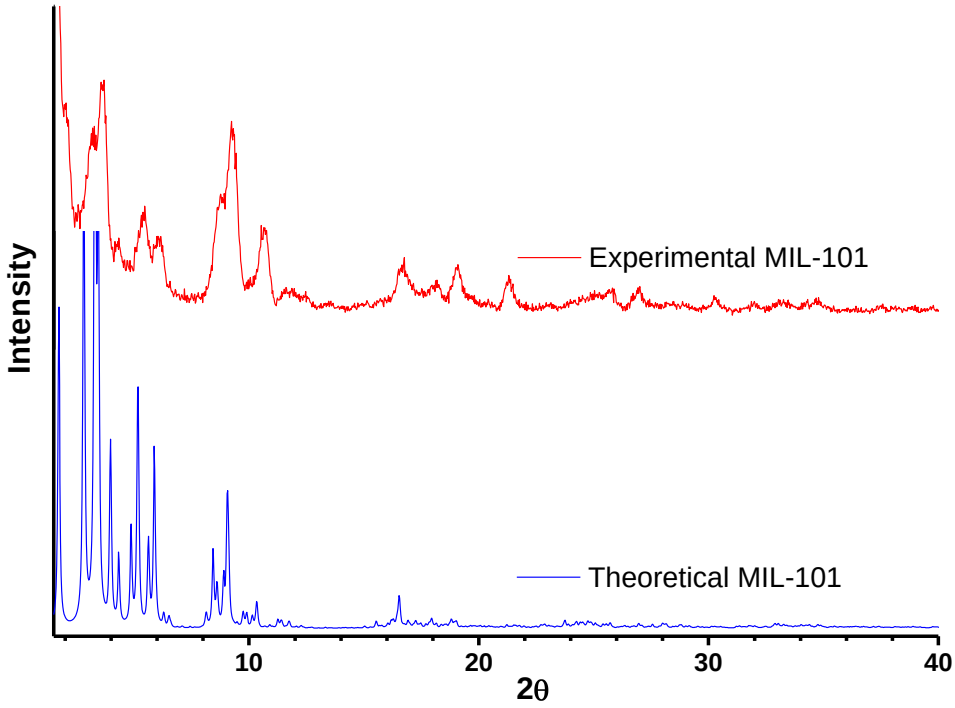

Figure 8. Comparison of the XRD pattern for calculated and synthesized MIL-101.

2.4.2. Nitrogen Adsorption Isotherm

An adsorption isotherm is the equilibrium uptake of a sorbate (for example as moles of adsorbate per gram of sorbent) measured at a constant temperature as a function of the concentration of the sorbate. For an adsorption from the gas phase, the adsorption is therefore measured as a function

of pressure. There are two main ways to measure the amount of adsorption- gravimetric and volumetric. In gravimetric methods the uptake is measured as the increase in weight of a sample as the adsorbate pressure is varied. This requires great accuracy in weighing. In volumetric method the change in pressure upon dosing known amounts of gas into a volume containing the sample are measured and the uptake calculated at the resultant equilibrium pressure. The adsorption of many vapors is most reliably performed gravimetrically, where condensation away from the sample has a negligible effect on the measurements. For low temperature and low pressure studies, however the volumetric method is preferred, because the sample is in contact with the walls of the sample container, itself immersed in the cryogenic bath. Heat transfer from the sample is, therefore, faster in the volumetric apparatus, and thermal equilibrium reached more quickly.

We have used the nitrogen adsorption branch from the N_2 isotherm to determine the Langmuir and BET surface areas and to calculate pore size distribution from Non-Local Density Functional Theory (NLDFT). Nitrogen physisorption measurements were measured using Quantachrome AUTOSORB-1-C/TCD instrument. Samples (~40-80 mg) were activated by degassing at 150 °C/10^{-5} torr for 12 hours. The nitrogen adsorption isotherm for MIL-101 is shown in Figure 9.

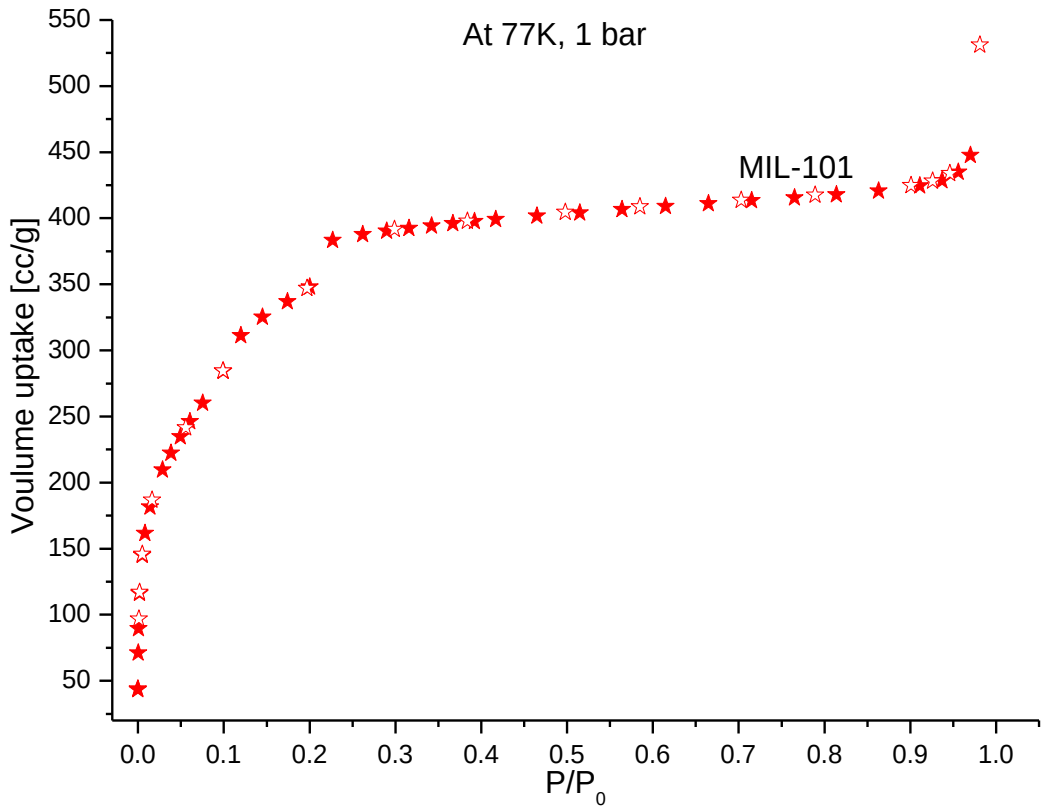

Figure 9. Nitrogen isotherm for MIL-101**,** filled (adsorption) and empty (desorption) symbol.

2.4.3. Surface Area

2.4.3.1. Langmuir Surface Area

Langmuir equation (Equation 2) was used to determine the surface area of synthesized MIL-101.

$$W/W_m = [C(P/P_o)]/\ 1 + C(P/P_o) \quad (2)$$

where W and W_m are the weight of adsorbate at some P/P_o and the weight in a monolayer. C is the energy of adsorption constant.

This equation could be written in a different form

$(P/P_o)/W = 1/CW_m + (P/P_o)/W_m$ where the slope $(1/W_m)$ is determined from the plot $(P/P_o)/W$ *vs* P/P_o.

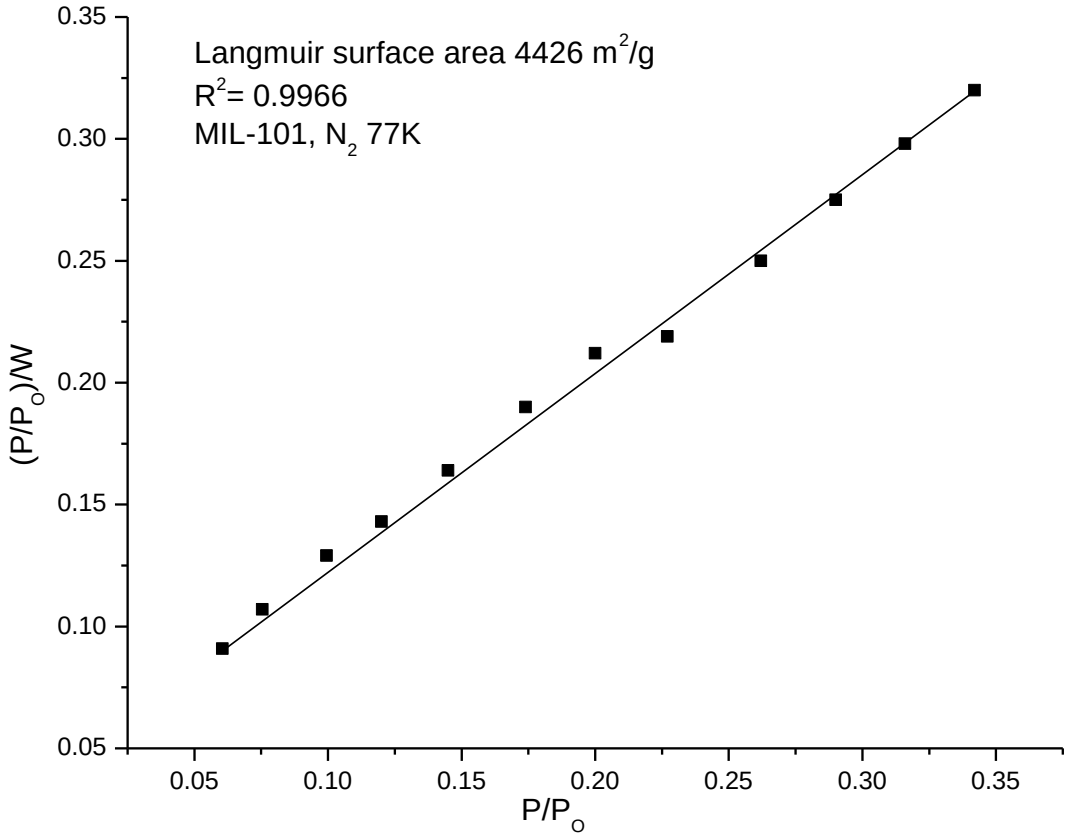

Figure 10. Langmuir surface area plot for MIL-101.

The Langmuir surface area calculated from nitrogen isotherm (Figure 10) for MIL-101 was found to be 4426 m^2/g.

2.4.3.2. The Brunauer-Emmett-Teller (BET)

Another method to determine surface area is the BET method which is an improvement over Langmuir method. Multipoint BET method was used to determine the surface area of MIL-101 using Equation 3:

$$1/ W((P_o/P) -1) = 1/W_mC + (C-1)/W_mC*(P/P_o) \qquad (3)$$

Where *W* is the weight of gas adsorbed at relative pressure, P/P_o, W_m is the weight of adsorbate constituting a monolayer of surface coverage. *C* is a BET constant related to energy of adsorption in the first adsorbed layer. From the BET equation above,

$1/W((P_o/P) - 1)$ *Vs* (P/P_o) was plotted, using nitrogen as the adsorbate. The calculated BET surface area for MIL-101 (Figure 11) was 2804 m^2/g.

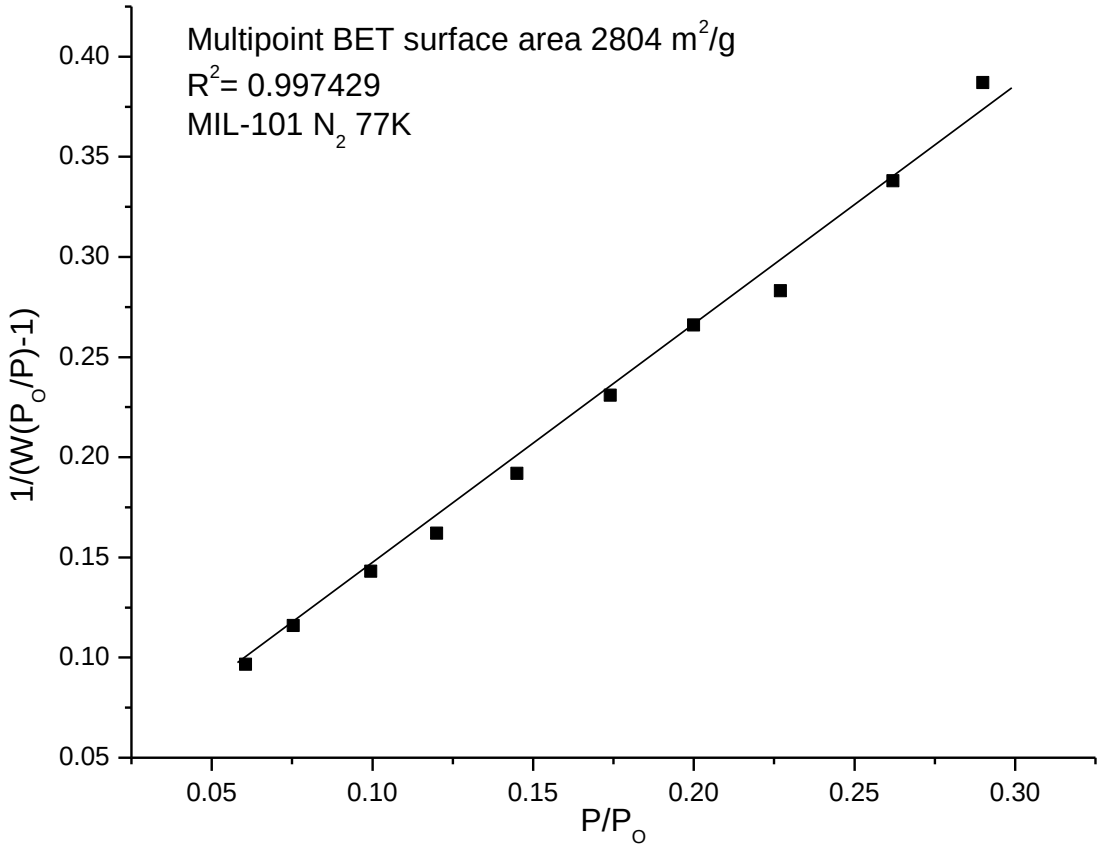

Figure 11. BET surface area plot for MIL-101.

2.4.4. DFT Pore Size Distribution

Density Functional Theory (DFT) was used to characterize the mesoporous nature of MIL-101. The quantachrome instrument operates on AS1WIN software. Hence the Quntachrome's data reduction software has a library of DFT and GCMC methods. Depending on the pore width range, the best model is picked. For our study NLDFT- N_2-silica adsorption branch kernel at 77

K based on cylindrical pore model was used. Cumulative volume verses pore width was plotted to find the pore volume distribution in MIL-101. It was shown that MIL-101 possesses two different pores of 26 Å and 32 Å and equal pore volumes of 0.13 cc/Å/g as shown in Figure 12.

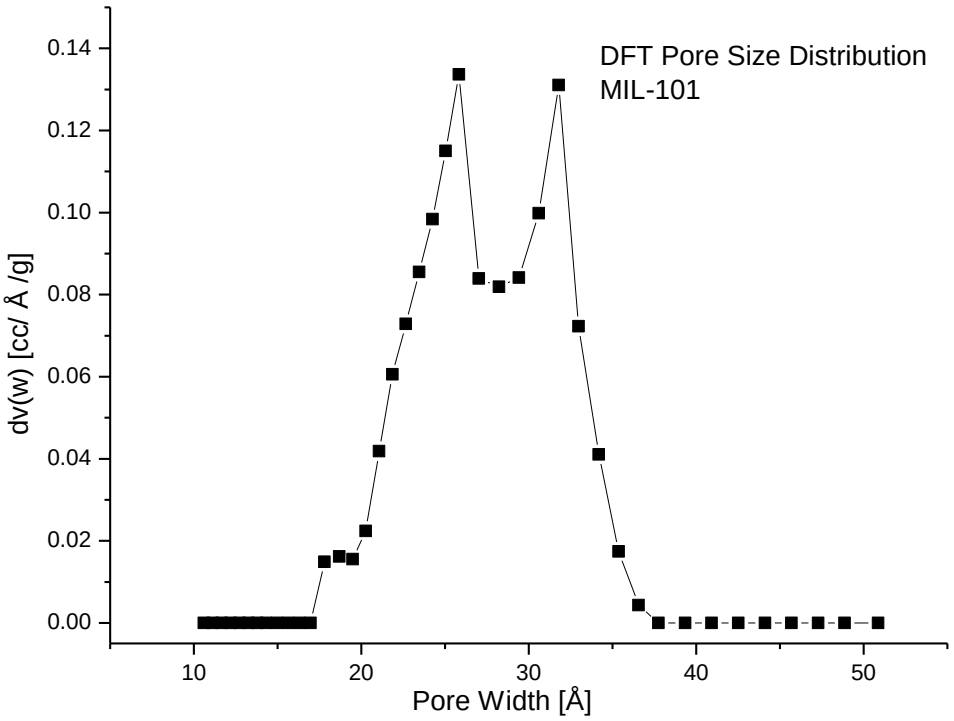

Figure 12. DFT pore size distribution plot for MIL-101.

2.4.5. Hydrogen Adsorption Isotherm.

Hydrogen Adsorption Isotherm at low pressure and 77K

We collected hydrogen adsorption isotherm on MIL-101 at 77 K and 0-1 bar using Quantachrome AUTOSORB-1-C/TCD instrument (Figure 13).

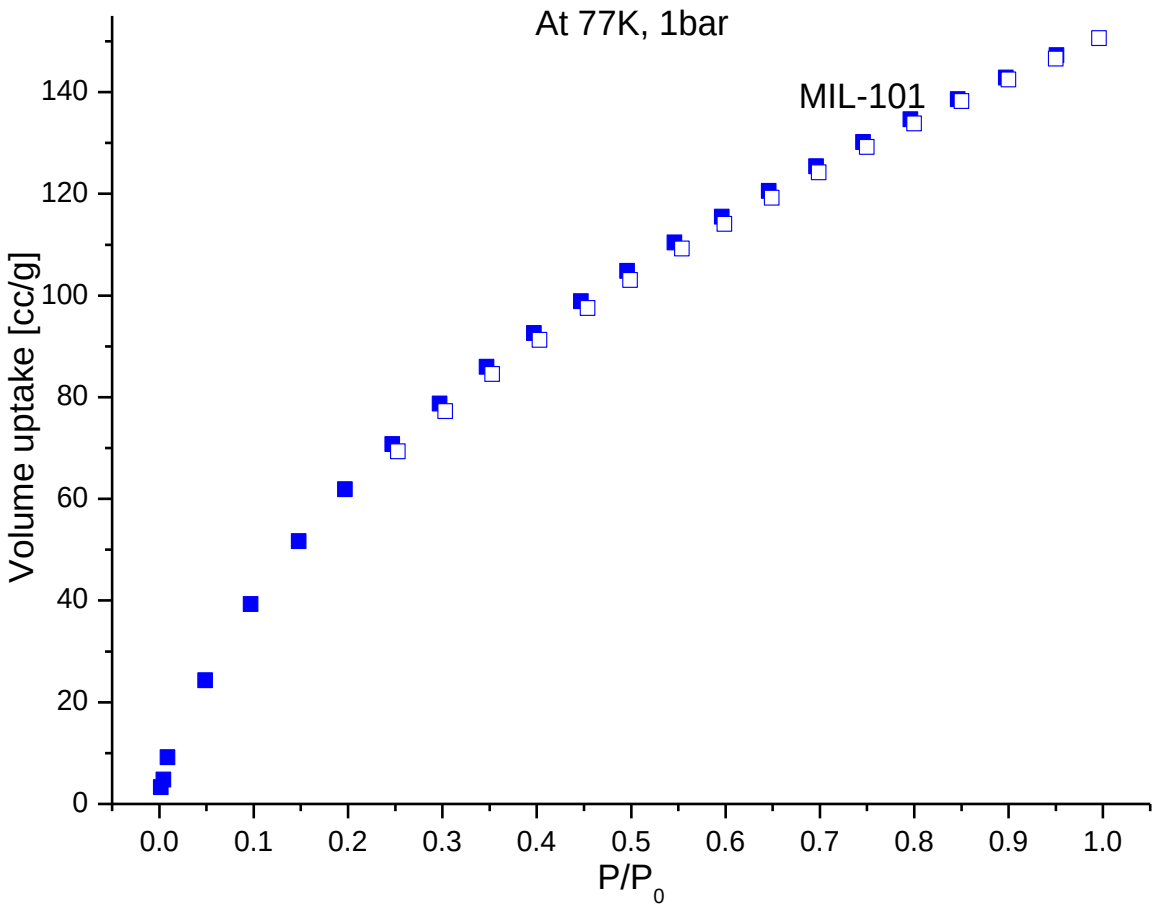

Figure 13. Hydrogen adsorption isotherm at 77 K and 1 bar in cc/g for MIL-101, filled (adsorption) and empty (desorption) symbol.

MIL-101 exhibits Type I isotherm, which typically shows high uptake at low pressure and a sharply defined maximum level of uptake as the internal pores are filled. The maximum uptake can be converted to pore volume per unit mass by assuming a density for the adsorbed nitrogen equal to that of gaseous nitrogen (1.25 g/cm^3) at that temperature. The first step corresponds to filling of micropores of the ST and the second step is due to the filling of the mesopores in MIL-101. Multilayer uptake is possible in mesoporous materials.

2.5. Hydrogen Adsorption on MIL-101

High hydrogen uptake of 6.1 wt% at 8 MPa and 77 K on MIL-101 has been reported by Férey. The hydrogen storage capacity in MIL-101 is 4.5 wt% at 40 bar.[55] In another study, MIL-101 has shown promising results of high hydrogen storage capacity of 3.75 wt% at 77 K and 2 MPa, but at room temperature the hydrogen uptake is 0.45 wt% at 2 MPa. In MIL-101 after activation by thermal or chemical treatment or combination of both, the weakly bound water and solvent molecules are easily removed and unsaturated metal sites are formed, and these open metal sites act as Lewis acid sites to increase the interaction with hydrogen (guest molecules) through changing its electronic density distribution. Hydrogen molecules has small kinetic diameter (2.89 Å) and interact with only high potential surface of the microporous windows is where the hydrogen molecules get adsorbed.[5] The location of hydrogen adsorped in MIL-101 mainly in the microporous super tetrahedron $(ST)^5$ formed from the trimers of chromium octahedron and benzene dicarboxylic acid (BDC) and probably at each corner near the trimers of chromium octahedron. The open metal (Cr) sites are not accounted because they are shielded by the leftover benzene dicarboxylic acid (BDC).[5] At temperature above critical point i.e. 32.97 K and 12.9 bar, it is difficult to adsorb hydrogen anywhere else in a multi layer way other than these four sites. However, taking into consideration the weak interaction of hydrogen into the pores in MIL-101, to require high potential surface to enhance hydrogen adsorption, large cavities may not be needed and also hydrogen molecules will not occupy the whole pore volume. Thus, MIL-101 has high surface area but the hydrogen surface densities are low. The adsorption enthalpy for MIL-101 is 10 kJ/mol. This is still lower than 15.1 kJ/mol required by DOE for storing hydrogen at ambient temperature. Though hydrogen adsorption in MIL-101 is reversible, requirement of high pressure and low temperature are the only drawbacks. In this study we try to

overcome these limitations by doping MIL-101 with Ni NPs. Our objective is to enhance hydrogen uptake by improving the isosteric heat of adsorption.

Table 2.1 Hydrogen uptake by MIL-101 at different temperature and pressure

H_2 Storage Capacity	**Temperature**	**Pressure**	**Reference**
3.75 wt%	77K	2 MPa	[4]
0.45 wt%	298 K	2 MPa	[4]
4.5 wt%	77 K	3 MPa	[4]
6.1 wt%	77 K	6 MPa	[56]
0.36 wt%	298 K	8.6 MPa	[56]
1.91 wt%	77 K	1 atm	[36]

Table 2.1 depicts hydrogen uptake by MIL-101 at different temperature and pressure range. At liquid nitrogen temperature and with increasing pressure of 0.101 MPa (1 atm), 2MPa, 3MPa, 6MPa MIL-101 shows an increasing trend of hydrogen uptake of 1.91 wt%, 3.75 wt%, 4.5 wt%, 6.1 wt% respectively. On the other hand, MIL-101 shows reverse trend at room temperature 298 K as opposed to liquid nitrogen temperature. With increase in pressure 2 MPa, 8.6 MPa hydrogen uptakes are 0.45 wt% and 0.36 wt%, respectively at room temperature.

Chapter 3

3.1. Doping Transition Metals in MOFs

One of the potential methods to increase hydrogen uptake at ambient condition is to dope porous materials with transition metals. Nickel has been reported for its capacity to improve hydrogen storage in porous material. MOFs physisorb molecular hydrogen through weak van der Waals interactions with heat of enthalpy generally about 4-10 KJ/mol. But low heats of adsorption lead to weak holding capacity of hydrogen to the surface under ambient conditions. Theoretical calculations show that 20-30 KJ/mol binding enthalpy would be needed for storing hydrogen at room temperature. One of the potential methods to increase hydrogen uptake at ambient condition is to dope porous material with transition metals as we have described earlier. It has been found that the heat of enthalpy could be increased as a result of Kubas interactions in which dihydrogen binds to coordination-active metal sites in η^2-H_2–M fashion. Due to the enhanced interaction of H_2, the pressure and temperature storage conditions would be more economically favorable.[57]

3.2. Doping MIL-101 with Nickel Nanoparticles

We have used the incipient wetness impregnation method to dope MIL-101 with two different concentrations of Ni NPs in order to investigate the impact of metal loading on hydrogen uptake and porosity of MIL-101. Our research group recently found that metal doping of MIL-101 (Cu, Pd, Pd-Cu) leads to lower surface areas as a result of pore clogging and pore

volume reduction which lower N_2 uptake.[51] To minimize this factor, we decided to target Ni concentrations lower than 5 wt% and investigate their impact on hydrogen uptake at 77 K and 298 K.

3.2.1. Wetness Impregnation Method:

In this doping method, the solid support (MIL-101 in our case) is wetted with a solution containing the metal precursor. The metal NPs precursor, typically a salt (metal nitrate, chloride) is dissolved in a minimum quantity of solvent to allow complete dissolution. The resulting solution is then added to the porous solid. The solvent is stirred overnight, and vacuum filtered the following day after metal reduction. The metal NPs formed during this method are found to be heterogeneously dispersed and exhibit different particle size depending on the metal type and loading, support, and reduction rate, among others. However the incipient wetness impregnation method often provides a broad NPs size distribution and is difficult to achieve a tuning of the particle size for particular applications. This is mainly due to the poor control over the growth of metal NPs. Nevertheless, this method remains widely employed in MOFs doping due to its simplicity and versatility.

In our experiments, samples of MIL-101 were suspended in deionized water. Then appropriate amounts of nickel (II) nitrate hexahydrate $Ni(NO_3)_2{:}6H_2O$ were added to the suspension while stirring for 24 hours. The resulting suspensions were then treated drop-by-drop with freshly prepared sodium borohydride (0.2 M) until the color changed from dark green to grayish black (Ni (II) to Ni (0)). The Ni@MIL-101 was then filtered through a medium fritt filter and washed with deionized water to remove unreacted nickel nitrate.

3.3. Characterization of Ni doped MIL-101

3.3.1. X-Ray Diffraction (XRD)

The PXRD patterns for the doped MIL-101 with 2 wt%, 5 wt% Ni and experimental undoped MIL-101 are shown in Figure 14. From the Figure it can be seen that MIL-101 material remains intact after doping and maintains its crystallinity.

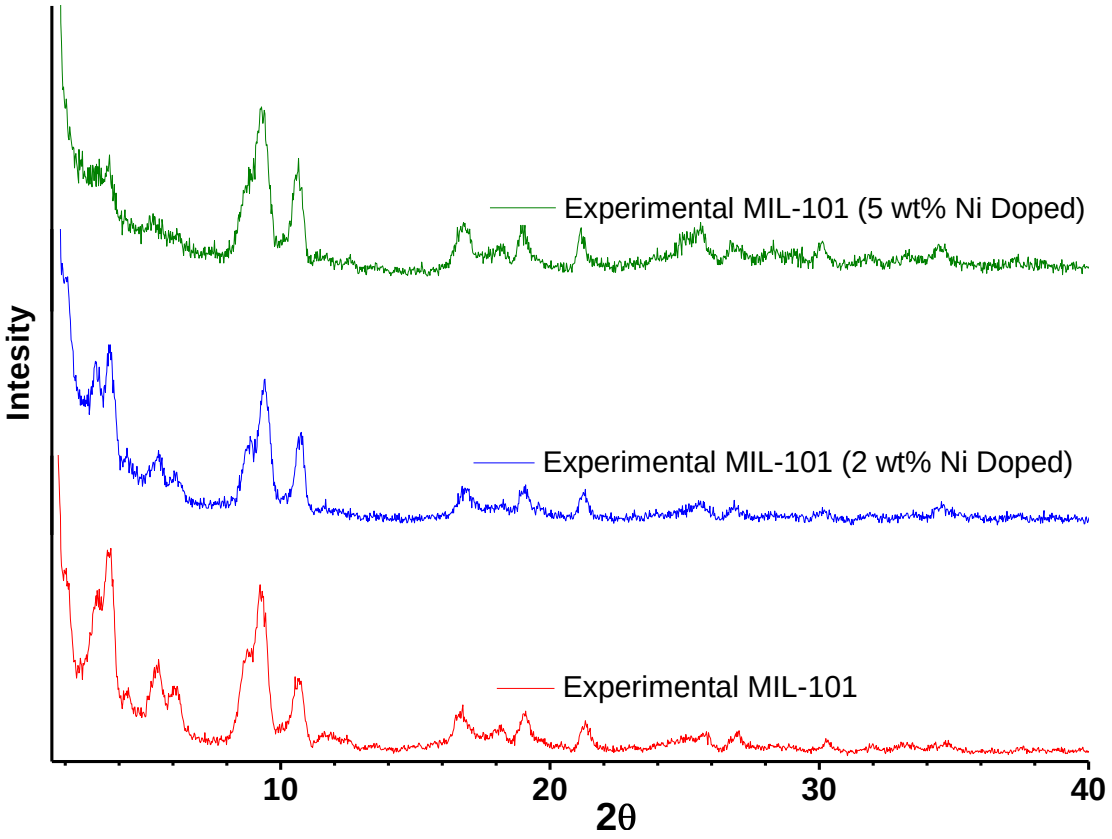

Figure 14. XRD pattern for as-synthesized MIL-101 and Ni-doped (2 wt% and 5 wt%) samples.

3.3.2. Transmission Electron Microscopy (TEM) Images

TEM was carried out using Joel JEM-1230 electron microscope operated at 120 kV equipped with Gatan Ultrascan 4000SP 4K X 4K CCD camera. Samples were prepared by suspending MIL-101 and its doped materials in ethanol. A drop of this suspension was coated on 300 mesh copper grid. The grid was air dried at room temperature. The TEM images of 2 wt% Ni doped mesoporous MIL-101 are shown in Figure 15. As shown in all of the images, small metal

particles are dispersed on the surface of MIL-101. It was estimated from the TEM images that the size of the Ni NPs are greater than 20 nm. Even though the images show that the Ni particles are on the surface, additional Ni NPs may also exist inside the MIL-101 cavities and their size should be smaller than the mesoporous cavity in MIL-101 which is about 3 nm. Therefore, it would be very difficult to determine the size of such NPs using low resolution TEM.

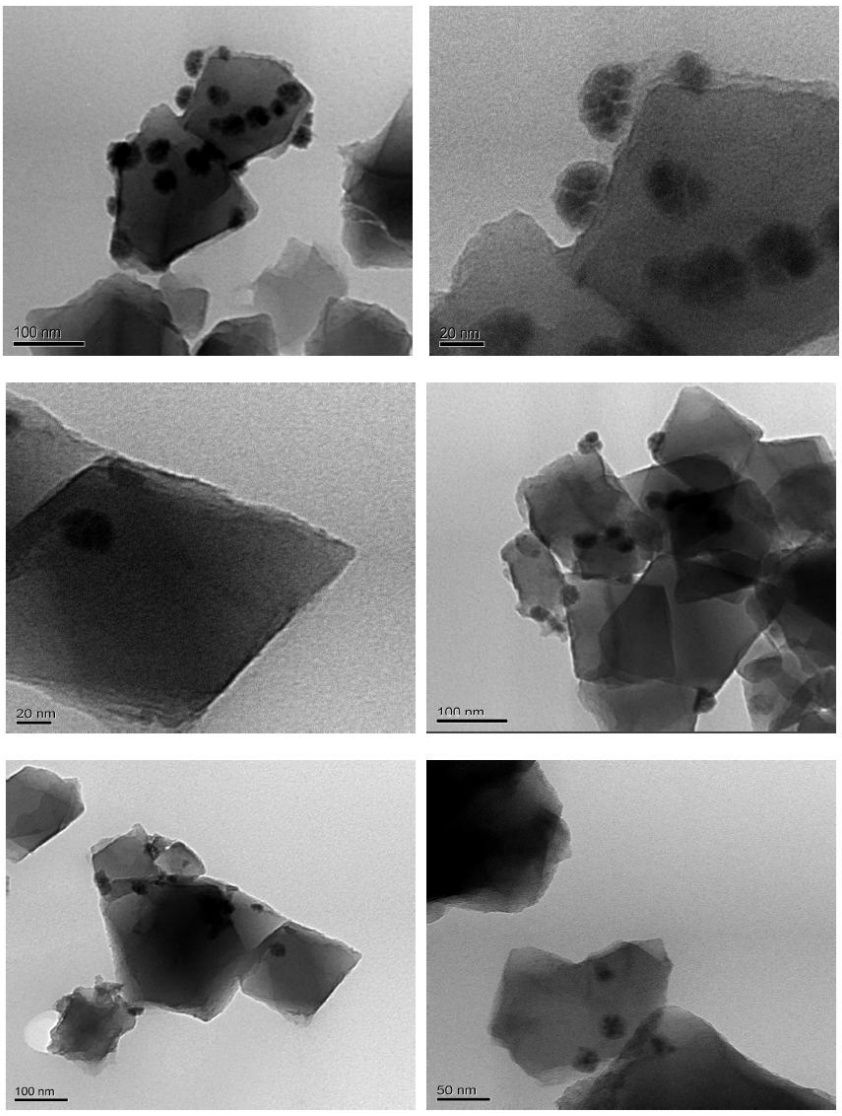

Figure 15. TEM images of Ni@MIL-101 (2 wt%) revealing the deposition of the metal NPs on the surface.

3.3.3. Inductively Coupled Plasma (ICP)

Inductively coupled plasma was used to determine the actual metal concentration in MIL-101 samples after filtration. Series of Ni standards (1, 2, 5, 10, 25, and 50 ppm) were prepared and made up to final volume of 50 ml with trace nitric acid 0.02 g of 2 wt% Ni doped MIL-101 and 5 wt% Ni doped MIL-101 was dissolved in aqua regia and sonicated and made to a final volume of 25 mililiters with trace nitric acid. The different concentrations of Ni were plotted against the intensity to make a calibration graph (Figure 16 and 17). Concentration of Ni in the MIL-101 sample was determined by solving the straight line equation. The intensity "y" for doped MIL-101 was plugged in the straight line equation and solved for "x" to get the concentration. The actual metal content for 2 wt% Ni doped MIL-101 was found to be 1.374 ± 0.0299 wt%. Similarly, the metal content for 5 wt% Ni doped MIL-101 was found to be 3.156 ± 0.0351. The lower metal contents are due to incomplete incorporation/reduction of Ni(II).

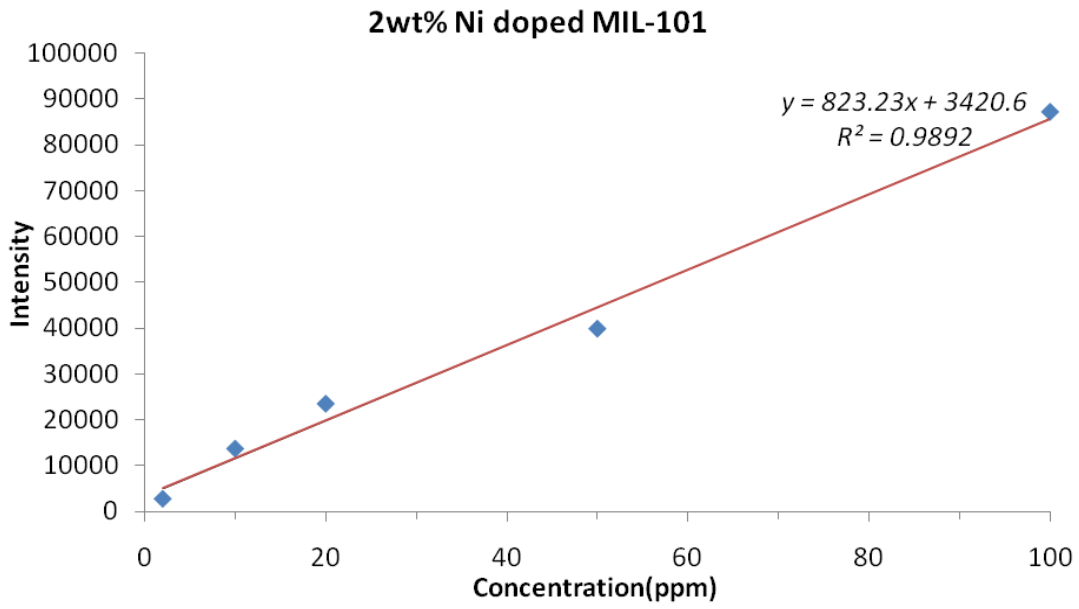

Figure 16. Calibration plot fom ICP experiment for 2 wt% Ni doped MIL-101

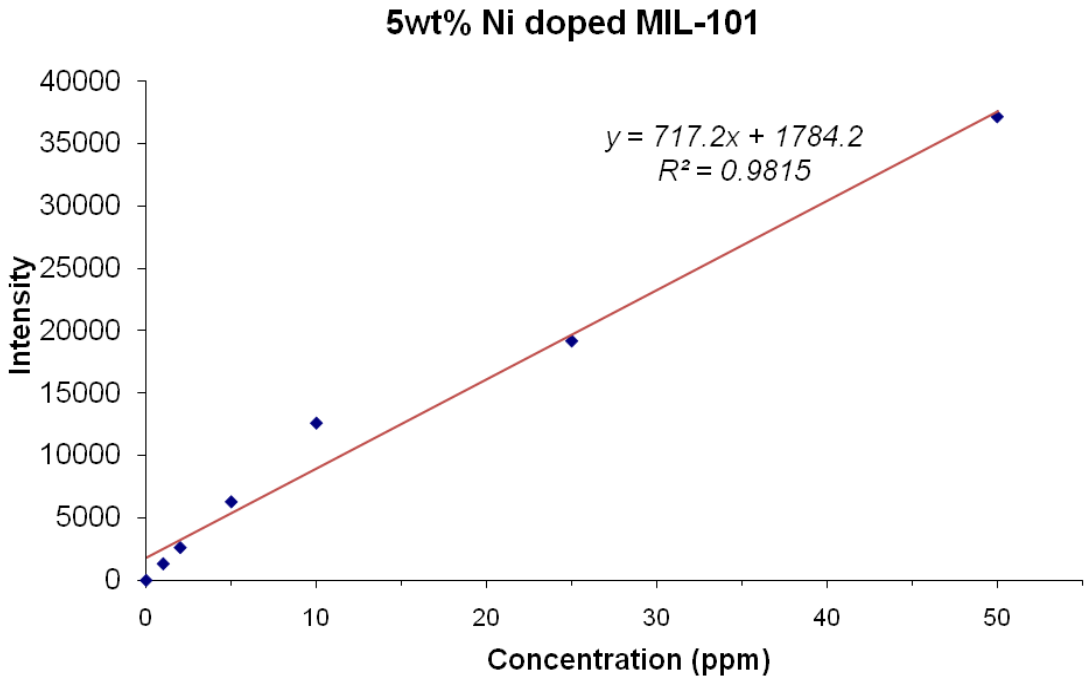

Figure 17. Calibration plot fom ICP experiment for 5 wt% Ni doped MIL-101

3.3.4. Nitrogen Adsorption Isotherm

Nitrogen adsorption was used to determine the Langmuir and BET surface areas and NLDFT pore size calculations. The nitrogen physisorption was measured using Quantachrome AUTOSORB-1-C/TCD instrument. Samples (40-80 mg) were loaded in quartz cell and activated at 150 ˚C/10^{-5} torr for 12 hours. The nitrogen adsorption isotherms for MIL-101 and Ni doped samples are given in Figure 18.

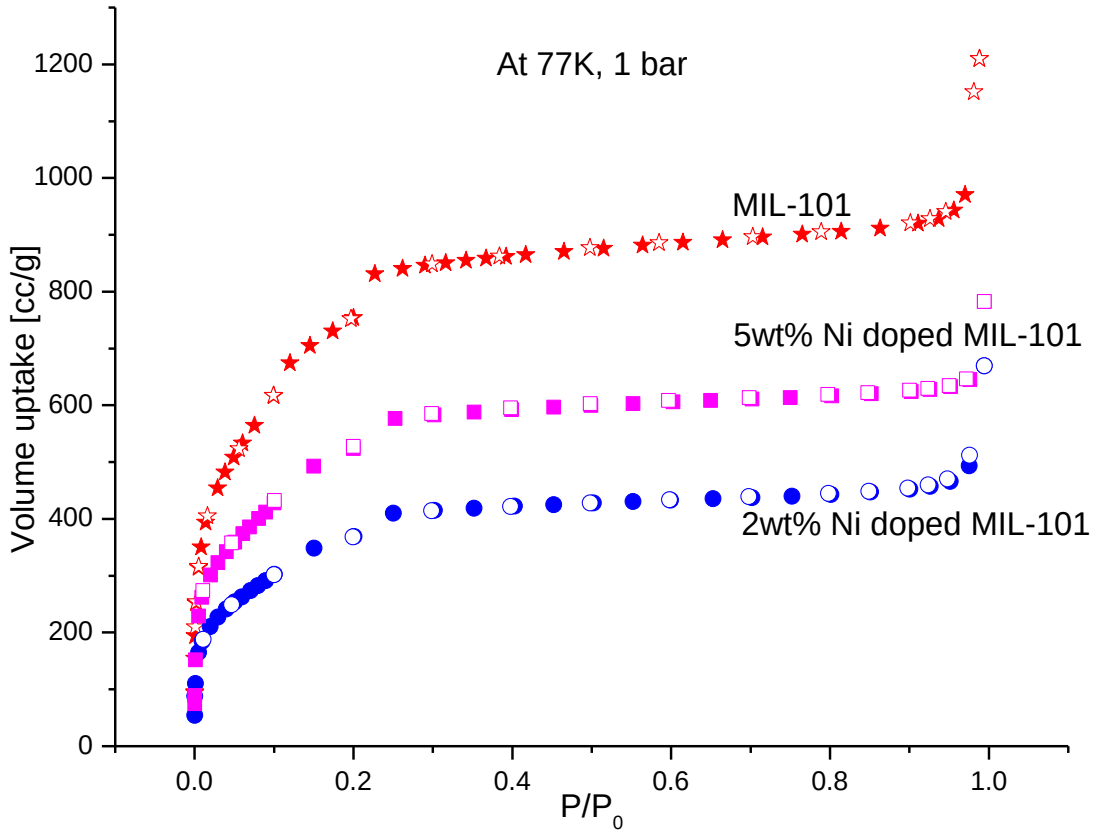

Figure 18. Nitrogen adsorption isotherms for undoped and doped MIL-101, filled (adsorption) and empty (desorption).

3.3.5. Surface Area

3.3.5.1. Langmuir Surface Area

MOFs are of high surface areas and are among the best known materials for physisorption of molecular hydrogen. Therefore it was important for us to determine the impact Ni doping on the surface area of MIL-101. The Langmuir surface area calculated from nitrogen isotherm (Figure 19) for 2 wt% Ni doped MIL-101 was found to be 2060 m^2/g which was less than the surface area of the undoped MIL-101, suggesting that Ni NPs exist inside the pores and on the surface as well. The Ni NPs restrict the access of MIL-101 cavities and thereby reduce its surface area.

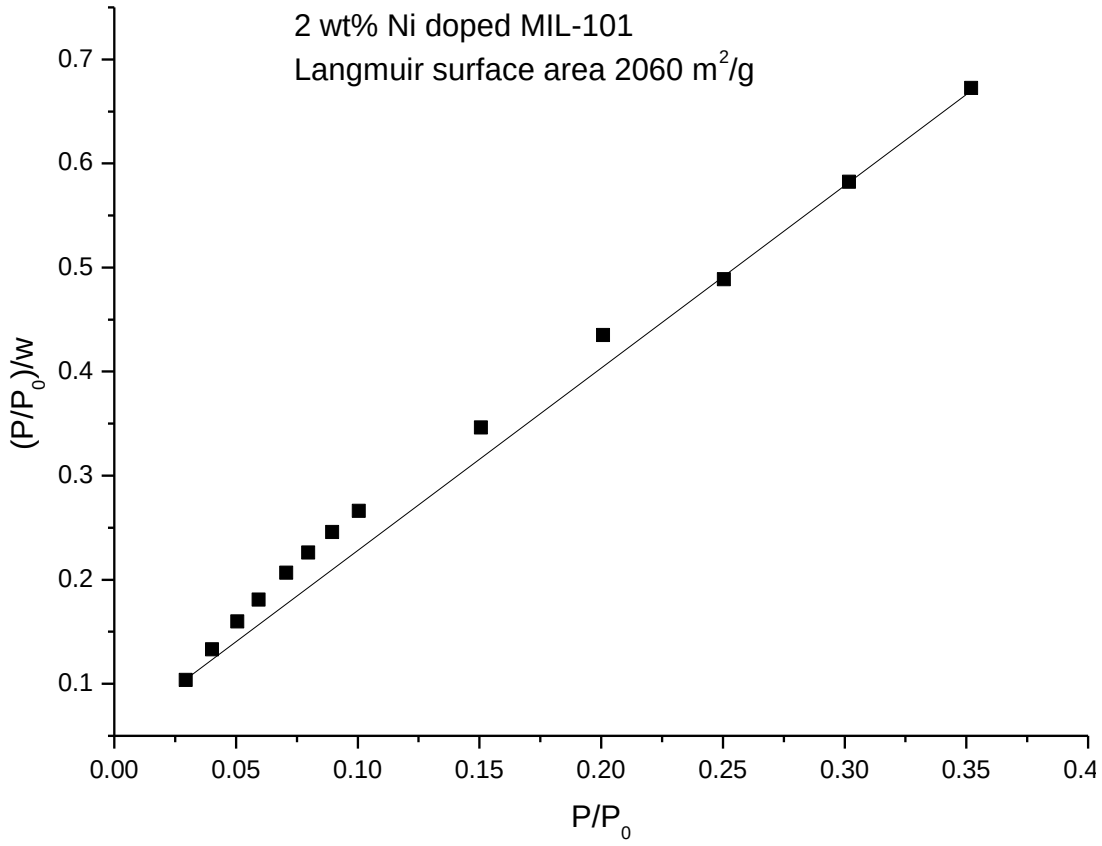

Figure 19. Langmuir surface area plot for 2 wt% Ni doped MIL-101.

In a similar fashion, the Langmuir surface area for 5 wt% Ni doped MIL-101 was lower (2990 m^2/g) than that of the parent MIL-101 as in Figure 20. Again, this may suggest that Ni NPs are clogging the pores and preventing their accessibility by nitrogen.

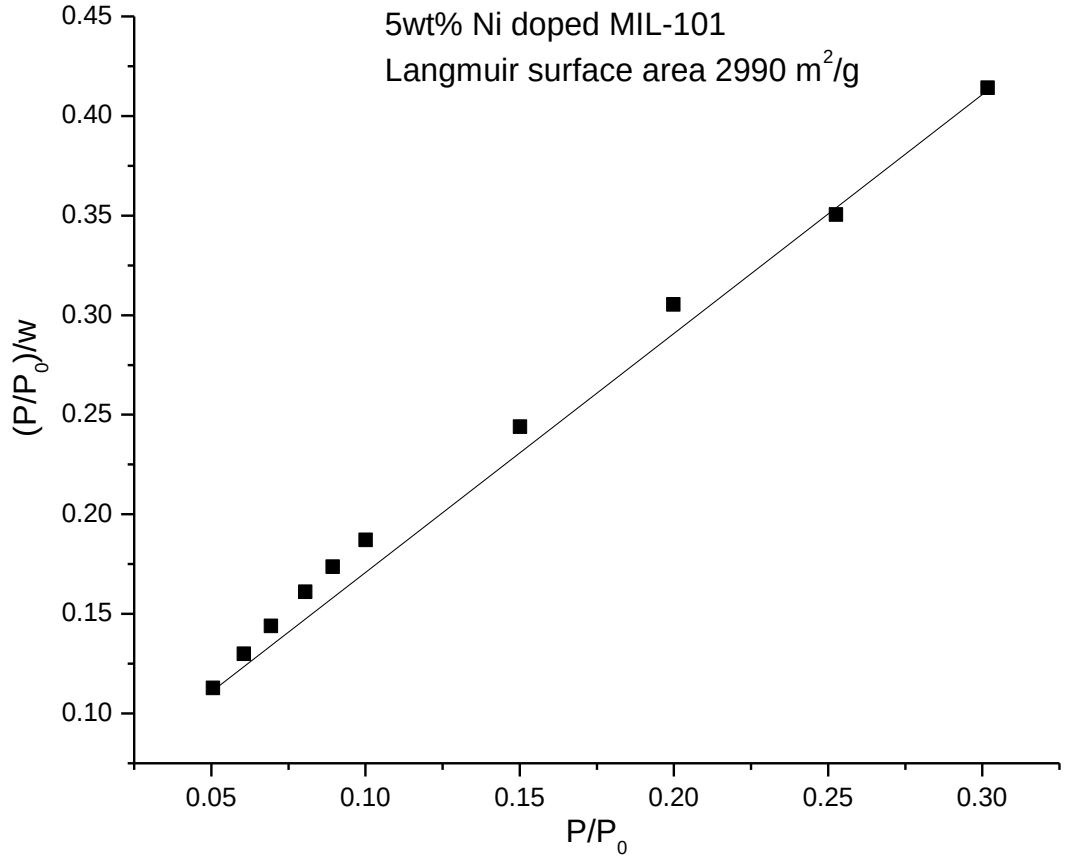

Figure 20. Langmuir surface area plot for 5 wt% Ni doped MIL-101.

3.3.5.2. The Brunauer-Emmett-Teller (BET) surface area

Multipoint BET method was also used to find out the surface area of the Ni doped MIL-101. The BET surface area calculated from nitrogen isotherm (Figure 21) for 2 wt% Ni doped MIL-101 found to be 1390 m^2/g which was less than that of the undoped MIL-101 as expected for similar reasons mentioned above.

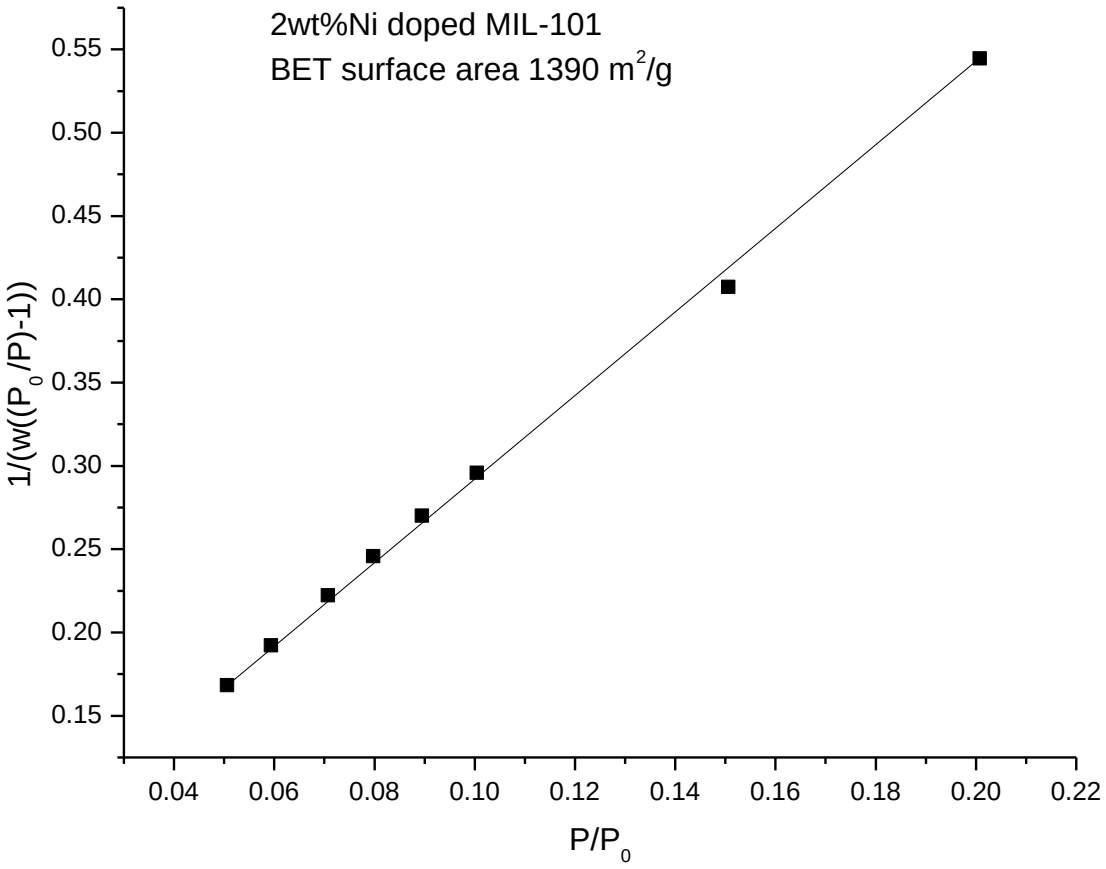

Figure 21. BET surface area plot for 2wt% Ni doped MIL-101

The BET surface area calculated from nitrogen isotherm (Figure 22) for 5 wt% Ni doped MIL-101 found to be 1980 m^2/g which was less than that of the undoped MIL-101, however more than 2 wt% Ni doped MIL-101 suggesting that Ni nanoparticles are mostly on the surface and less inside the pore.

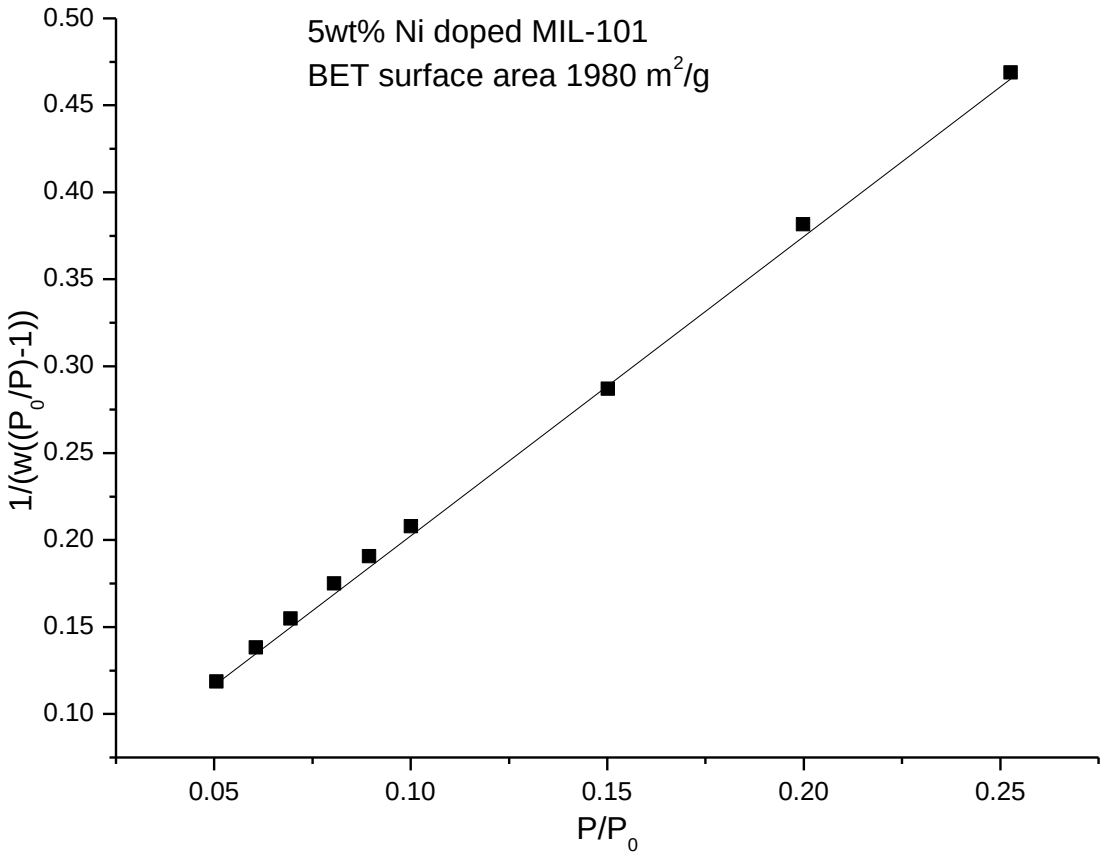

Figure 22. BET surface area plot for 5 wt% Ni doped MIL-101.

3.3.6. DFT Pore Size Distribution

The impact of metal inclusion inside the cavity of MIL-101 can easily be investigated using several methods which allow for pore size distribution calculation. Among these methods is NLDFT (Non Local Density Function Theory). After doping with 2 wt% Ni, pore volumes of MIL-101 cavities were decreased as seen in Figure 23. Noteworthy was that the volume of the larger pore (0.055 cc/Å/g) decreased more than that of the smaller pore (0.07 cc/Å/g) as seen in Figure 23. This can be explained as a result of more Ni NPs being accommodated in the larger cages. For the 5wt% doped MIL-101, the pore volume for larger pore and smaller pore were 0.07 cc/Å/g and 0.10 cc/Å/g respectively, as shown in Figure 24. This suggests that as the Ni

concentration was increased, the Ni NPs formed aggregates which may impact both surface area and pore volume.

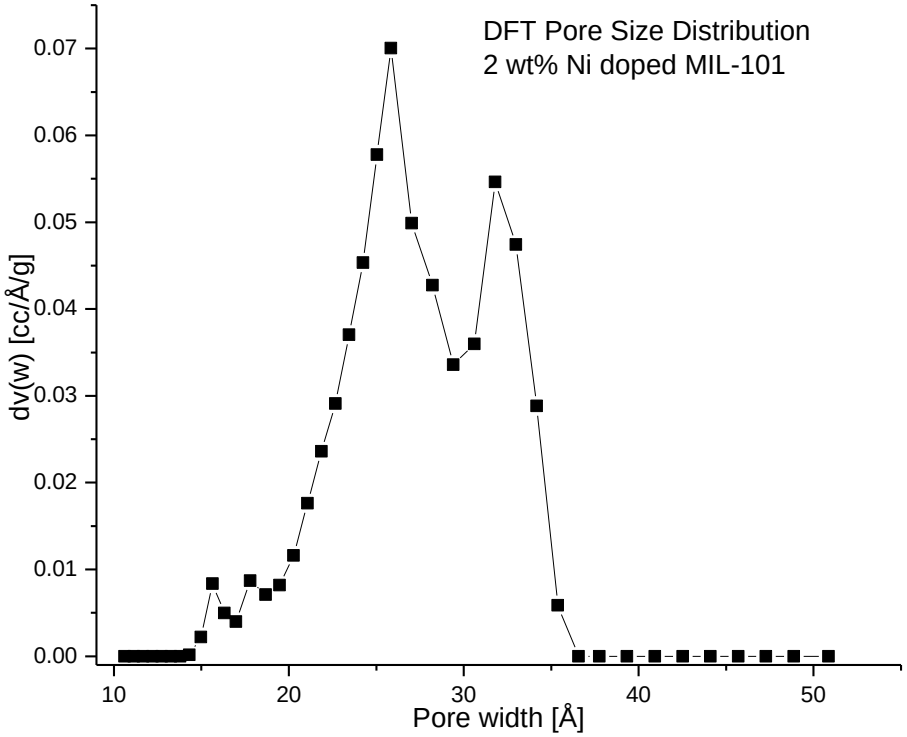

Figure 23. DFT pore size distribution plot for 2 wt% Ni doped MIL-101.

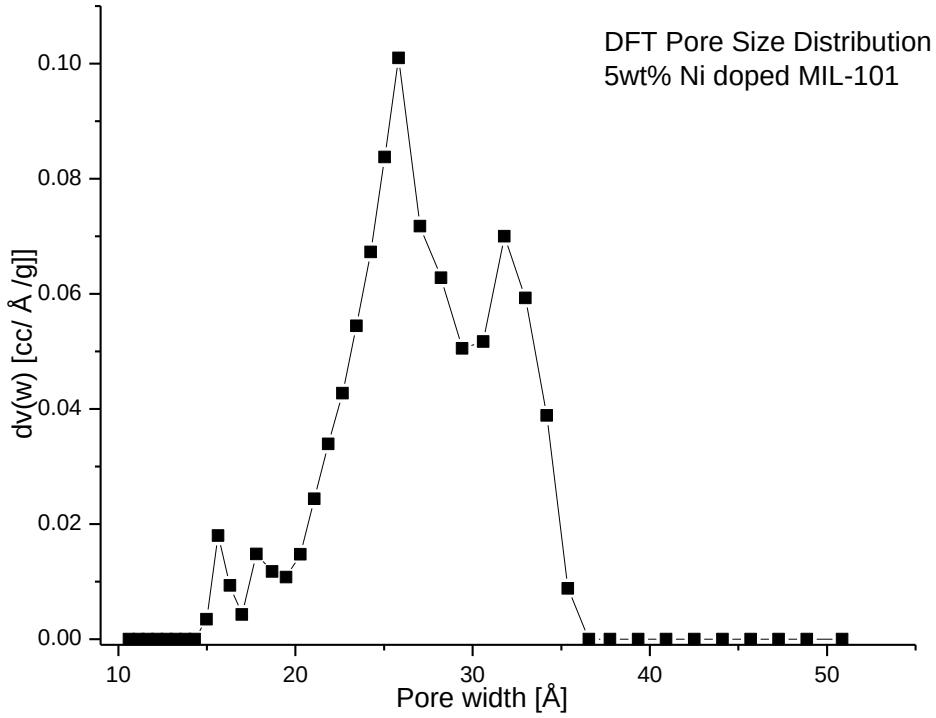

Figure 24. DFT pore size distribution plot for 5 wt% Ni doped MIL-101.

3.3.7. Hydrogen Uptake

3.3.7.1. Hydrogen Uptake at 0-1 bar and 77 K.

The experimental data for the hydrogen uptake by Ni doped MIL-101 and the parent material are presented in Figure 25 and Figure 26. The data show that the hydrogen adsorption amounts for 5 wt% Ni doped MIL-101 are higher than that of 2 wt% MIL-101 at 77 K and 1 bar shown in Figure 25. The wt% of hydrogen uptake for MIL-101 at 77 K and 1 bar is 1.3 wt%. This value is higher than the uptake by Ni-doped samples (5 wt% Ni doped MIL-101: 0.85 wt%; 2 wt% Ni doped MIL-101: 0.75 wt%) shown in Figure 26. It was surprising that the Ni doped MIL-101 samples exhibit a lower hydrogen uptake than the parent material. One possible explanation would be the impact of doping on surface area or the formation of oxide layer on the surface of

the Ni NPs which could prevent their interaction with hydrogen. Both possibilities would have negative impact on hydrogen uptake.

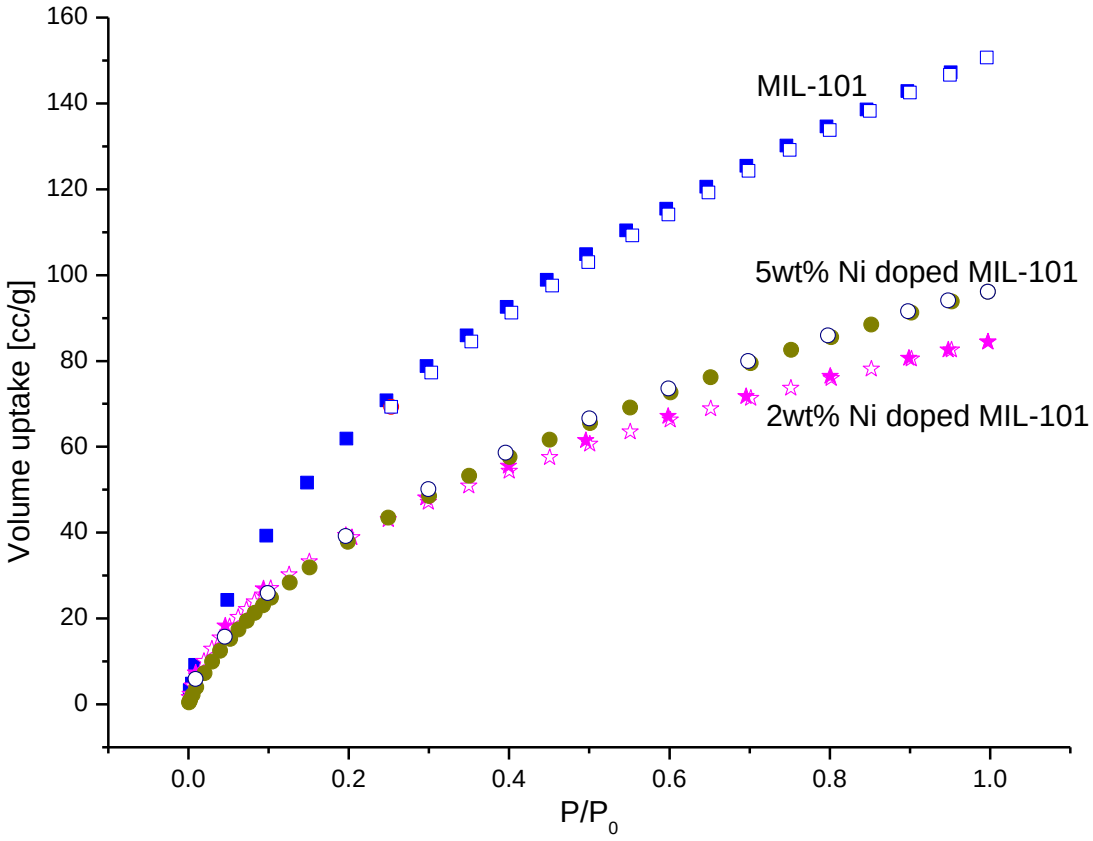

Figure 25. Hydrogen adsorption isotherm at 77 K and 1 bar in cc/g for undoped and Ni doped MIL-101, filled (adsorption) and empty (desorption) symbol.

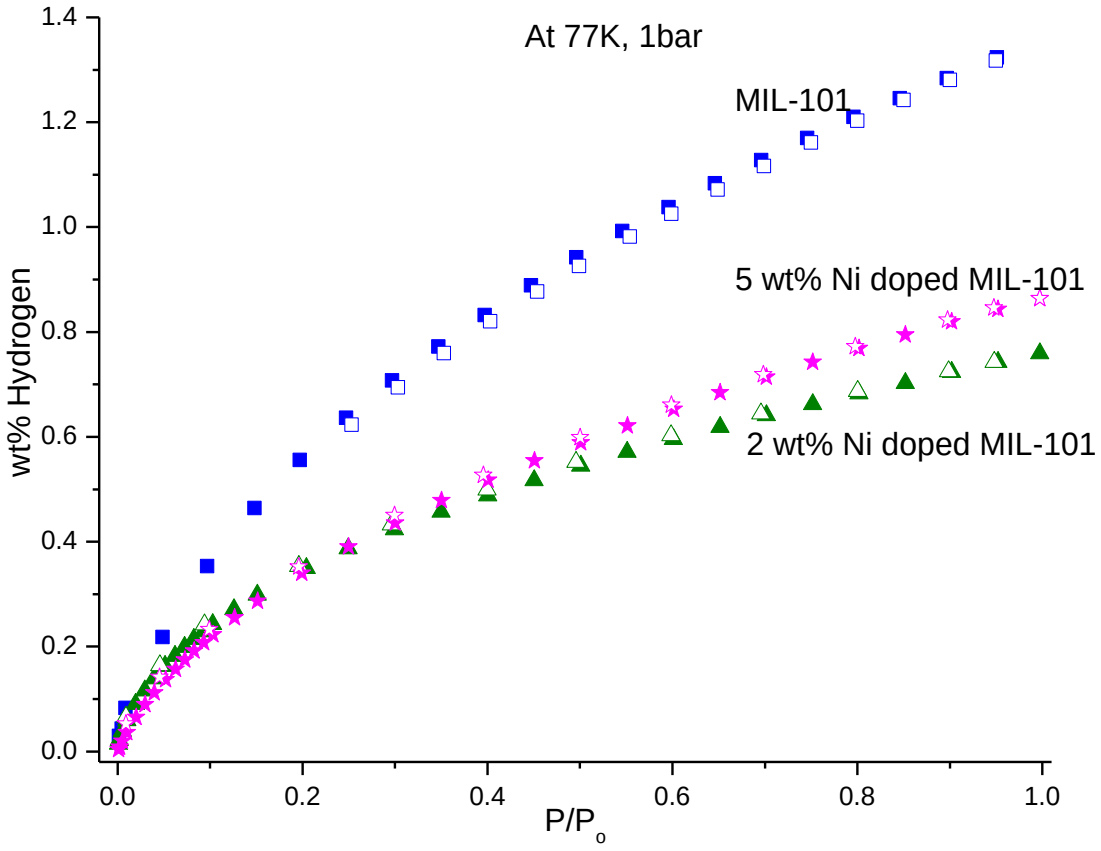

Figure 26. Hydrogen adsorption isotherm at 77 K and 1 bar in wt% for undoped and Ni doped MIL-101, filled (adsorption) and empty (desorption) symbol.

3.3.7.2. Hydrogen Uptake at 0-1 bar and 298K

To investigate the impact of Ni doping on hydrogen uptake at ambient conditions (1-0 bar, 298 K) we have collected hydrogen uptake isotherms at room temperature. The rationale behind these experiments was to determine whether Ni-doped samples would outperform the parent material in the absence of cooling effects. In this study, MIL-101 shows 0.00085 wt% of hydrogen uptake at 298 K and 1 bar. In contrast, 5 wt% Ni doped MIL-101 and 2 wt% Ni doped MIL-101 stored 0.00052 wt% and 0.00040 wt% of hydrogen, respectively shown in Figure 28. Again, the hydrogen uptake was higher for undoped MIL-101 indicating that nickel NPs plays a negative role in hydrogen uptake.

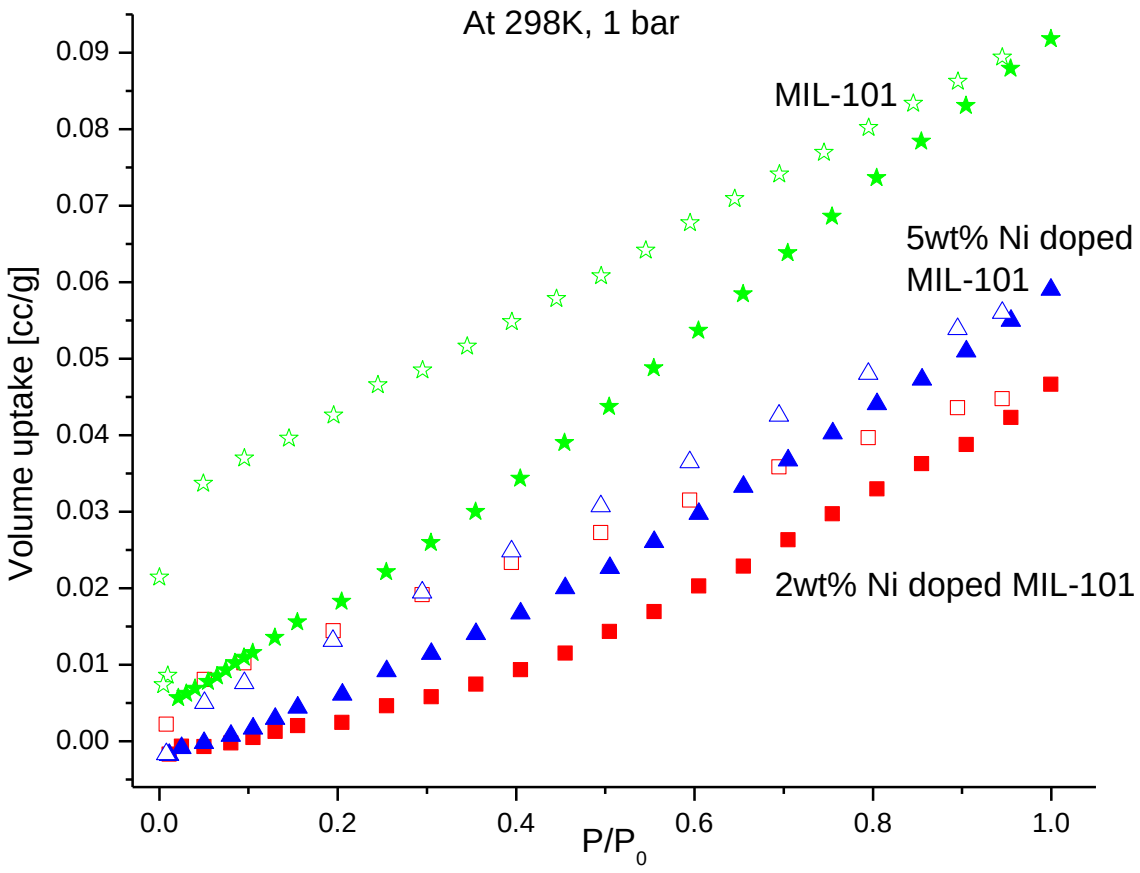

Figure 27. Hydrogen adsorption isotherm at 298 K and 1 bar in cc/g for Ni doped MIL-101, filled (adsorption) and empty (desorption) symbol.

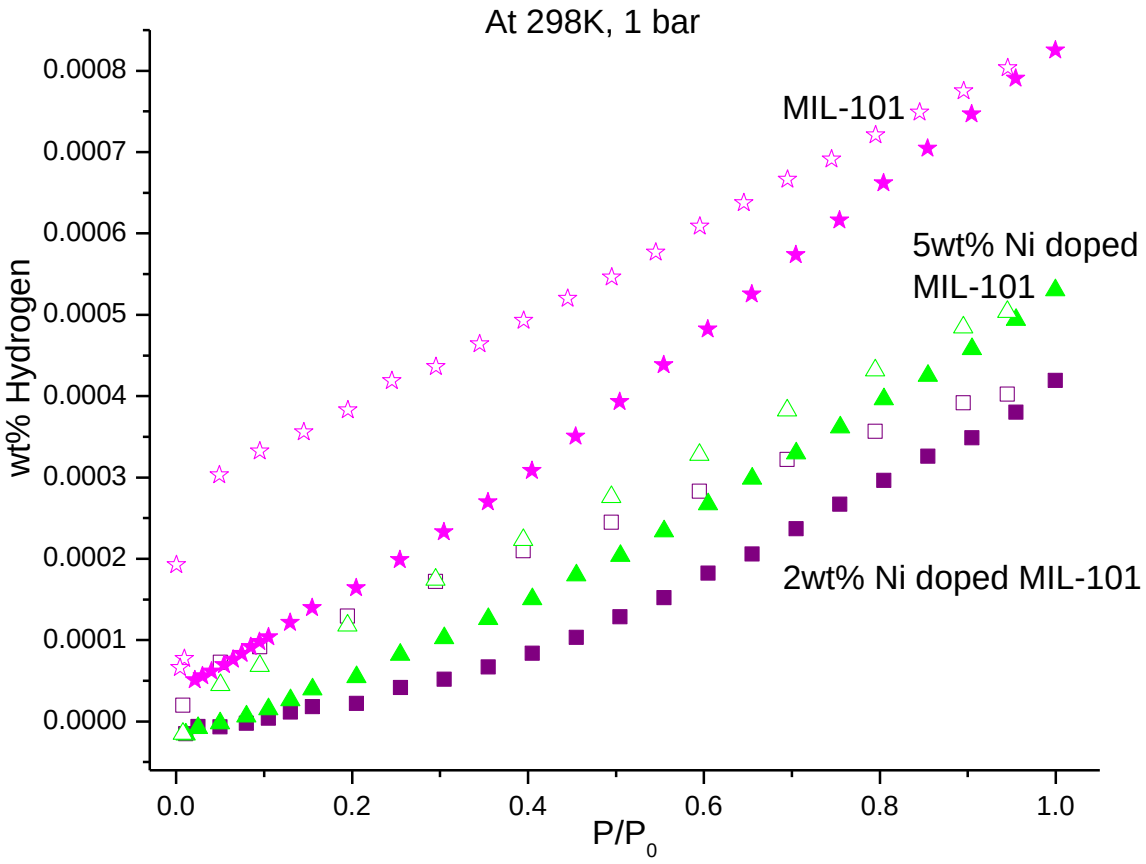

Figure 28. Hydrogen adsorption isotherm at 298 K and 1 bar for wt% for Ni doped MIL-101, filled (adsorption) and empty (desorption) symbol.

Conclusions

From the results described in the previous section, we have found that nickel doping of MIL-101 resulted in a significant reduction in surface area and lower hydrogen uptake despite of the low Ni NPs loading. All materials, MIL-101 and its Ni doped analogs have modest hydrogen uptake at low pressure and 77 to 298 K which remain far from DOE targets set for 2010 and 2015 (by 2010, develop on-board hydrogen storage achieving 2 kWh/kg (6 wt%), 1.5 kWh/L and by 2015, 3 kWh/kg (9 wt%), 2.7 kWh/L. Another possibility for the low hydrogen uptake might be the formations of NiO on the surface of Ni NPs. Metal oxide layers prevent hydrogen interaction with metal atoms on the surface, thus reducing spillover and Kubas interaction. We suggest that extra research is needed to investigate the chemical nature of Ni NPs using XPS. This objective is beyond the scope of our study.

List of References

1. Tans, P., NOAA/ESRL (www.esrl.noaa.gov/gmd/ccgg/trends/)

2. Schlapbach, L.; Zuttel, A., *Nature* **2001,** *414*, 353-358.

3. Yaghi, O. M.; O'Keeffe, M.; Ockwig, N. W.; Chae, H. K.; Eddaoudi, M.; Kim, J., *Nature* **2003,** *423*, 705-714.

4. Ferey, G.; Mellot-Draznieks, C.; Serre, C.; Millange, F.; Dutour, J.; Surble, S.; Margiolaki, I., *Science* **2005,** *309*, 2040-2042.

5. Xiao, B.; Yuan, Q., *Particuology* **2009,** *7*, 129-140.

6. Yang, Q.; Zhong, C., *J. Phys. Chem. B* **2006,** *110* (2), 655-658.

7. Lueking, A. D.; Yang, R. T., *Appl. Catal. A* **2004,** *265*, 259-268.

8. Kubas, G. J.; Ryan, R. R.; Swanson, B. I.; Vergamini, P. J.; Wasserman, H. J., *J. Am. Chem. Soc* **1984,** *106*, 451-452.

9. Houghton, J. T.; Ding, Y.; Griggs, D. J.; Noguer, M.; Linden, P. J. V. D.; Dai, X.; Maskell, K.; Johnson, C. A., *Climate Change 2001: The Scientific Basis*. Cambridge University Press: 2001.

10. New Horizens for Hydrogen. U.S. Department of Energy, Ed. DOE Hydrogen program: 2008.

11. Hydrogen Storage. U.S. Department of Energy, Ed. DOE Hydrogen Program: 2008.

12. Gross, K. J.; Carrington, K. R.; Barcelo, S.; Karkamkar, A.; Purewal, J.; Parilla, P. *Recommended Best Practices for the Characterization of Storage Properties of Hydrogen Storage Materials*; U.S. D.O.E.: 2009.

13. Hydrogen - An Overview. U.S. Department of Energy, Ed. 2008.

14. Eberle, U.; Felderhoff, M.; Schuth, F., *Angew. Chem. Int. Ed* **2009,** *48*, 2-25.

15. Zhao, D.; Yuan, D.; Zhou, H. C., *Energy. Environ. Sci* **2008,** *1*, 222-235.

16. Hirscher, M.; Panella, B., *Scripta Materialia* **2007,** *56*, 809-812.

17. (a) Dillon, A. C.; Jones, K. M.; Bekkedahl, T. A.; Kiang, C. H.; Bethune, D. S.; Heben, M. J., *Nature* **1997,** *386*, 377-379; (b) Anson, A.; Callejas, M. A.; Benito, A. M.; Maser, W. K.; Izquierdo, M. T.; Rubio, B.; Jagiello, J.; Thommes, M.; Parra, J. B.; Martinez, M. T., *Carbon* **2004,** *42*, 1243-1248.

18. Kajura, H.; Tsutsui, S.; Kadono, K.; Ata, M.; Murakami, Y., *Appl. Phys. Lett* **2003,** *82*, 1105-1107.

19. Shao, X.; Wang, W.; Xue, R.; Shen, Z., *J. Phys. Chem. B* **2004,** *108*, 2970-2978.

20. Fu, R.; Baumann, T. F.; Cronin, S.; Dresselhaus, G.; Dresselhausand, M. S.; Satcher, J. H., *Langmuir* **2005,** *21*, 2647-2651.

21. Gadiou, R.; Saadallah, S. E.; Piquero, T.; David, P.; Permentier, J.; Vix-Gutrel, C., *Microporous Mesoporous Mater* **2005,** *79*, 121-128.

22. Xia, Y.; Mokaya, R., *J. Phys. Chem. C* **2007,** *111*, 10035-10039.

23. Weitkamp, J.; Fritz, M.; Ernst, S., *Int J Hydrogen Energy* **1995,** *20*, 967-970.

24. Tranchemontagne, D. J.; Mendoza-Cortes, J. L.; O'Keeffe, M.; Yaghi, O. M., *Chem. Soc. Rev* **2009,** *38*, 1257-1283.

25. Mandoki, N. T.; Dentzer, J.; Piquero, T.; Saadallah, S.; David, P.; Guterl, C. V., *Carbon* **2004,** *42*, 2735-2777.

26. Kajiura, H.; Tsutsui, S.; Kadono, K.; Kakuta, M.; Ata, M., *Appl. Phys. Lett* **2003,** *82*, 1105.

27. Pang, J.; Hampsey, J. E.; Wu, Z.; Hu, Q.; Lu, Y., *Appl. Phys. Lett* **2004,** *85*.

28. Ma, S.; Zhou, H. C., *Chem. Commun.* **2010,** *46*, 44-53.

29. Liu, Y.; Kabbour, H.; Brown, C. M.; Neumann, D. A.; Ahn, C. C., *Langmuir* **2008,** *24*, 4772-4777.

30. Vitillo, J. G.; Regli, L.; Chavan, S.; Ricchiardi, G.; Spoto, G.; Dietzel, P. D. C.; Bordiga, S.; Zecchina, A., *J. Am. Chem. Soc* **2008,** *130*, 8386-8396.

31. Zielinski, M.; Wojcieszak, R.; Monteverdi, S.; Mercy, M.; Bettahar, M. M., *Int. J. Hydrogen Energy* **2007,** *32*, 1024-1032.

32. Saha, D.; Deng, S., *Langmuir* **2009,** *25* (21), 12550-12560.

33. Kim, H. S.; Lee, H.; Han, K. S.; Kim, J. H.; Song, M. S.; Park, M. S.; Lee, J. Y.; Kang, J. K., *J. Phys. Chem. B* **2005,** *109*, 8983-8986.

34. White, R. J.; Luque, R.; Budarin, V. L.; Clark, J. H.; Macquarrie, D. J., *Chem. Soc. Rev* **2009,** *38*, 481-494.

35. Hoang, T. K. A.; Antonelli, D. M., *Adv. Mater* **2009,** *21*, 1787-1800.
36. Li, Y.; Yang, R. T., *AIChE Jounal* **2008,** *54* (1), 269-279.

37. Li, Y.; Yang, R. T., *J. Am. Chem. Soc* **2006,** *128*, 8136-8137.

38. Niu, J.; Rao, B. K.; Jena, P., *Phys. Rev. Letts* **1992,** *68*, 2277.

39. Niu, J.; Rao, B. K.; Jena, P., *Phys. Rev. B* **1995,** *51*, 4475.

40. Niu, J.; Rao, B. K.; Khanna, S. N.; Jena, P., *Chem. Phys. Lett.* **1994,** *230*, 299-305.

41. Rao, B. K.; Jena, P., *Europhysics Letters* **1992,** *20*, 307-312.

42. Mueller, U.; Schubert, M.; Teich, F.; Puetter, H.; Schierle-Arndt, K.; Pastre, J., *J. Mater. Chem* **2006,** *16* (7), 626-636.

43. Lin, Z.; Wragg, D. S.; Morris, R. E., *Chem. Commun.* **2006,** *19*.

44. Lin, X.; Jia, J.; Zhao, X.; Thomas, K. M.; Blake, A. J.; Walker, G. S., *Angew. Chem. Int. Ed* **2006,** *45* (44), 7358-7364.

45. Sonnauer, A.; Hoffmann, F.; Froba, M.; Kienle, L.; Duppel, V.; Thommes, M.; Serre, C.; Ferey, G.; Stock, N., *Angew. Chem. Int. Ed* **2009,** *48*, 1-5.

46. Henschel, A.; Gedrich, K.; Kraehnert, R.; Kaskel, S., *Chem. Commun.* **2008**, 4192-4194.

47. Lebedev, O. I.; Millange, F.; Serre, C.; Tendeloo, G. V.; Ferey, G., *Chem. Mater* **2005,** *17*, 6525-6527.

48. Ferey, G., *Chem. Soc. Rev* **2008,** *37*, 191-214.

49. Hwang, Y. K.; Hong, D. Y.; Chang, J. S.; Jhung, S. H.; Seo, Y. K.; Kim, J.; Vimont, A.; Daturi, M.; Serre, C.; Ferey, G., *Angew. Chem. Int. Ed* **2008,** *47*, 1-6.

50. Kim, J.; Bhattacharjee, S.; Jeong, K. E.; Jeong, S. Y.; Ahn, W. S., *Chem. Commun.* **2009**, 3904-3906.

51. El-Shall, M. S.; Abdelsayed, V.; Khder, A.; Hassan, H.; El-Kaderi, H.; Reich, T., *J. Mater.Chem.* **2009,** *19*, 7625-7631.

52. Maksimchuk, N. V.; Timofeeva, M. N.; Melgunov, M. S.; Shmakov, A. N.; Chesalov, Y. A.; Dybtsav, D. N.; Fedin, V. P.; Kholdeeva, O. A., *J. Catal.* **2008,** *257*, 315-323.

53. Hwang, Y. K.; Hong, D. Y.; Chang, J. S.; Seo, H.; Yoon, M.; Kim, J.; Jhung, S. H.; Serre, C.; Ferey, G., *Appl. Catal. A* **2009,** *358*, 249-253.

54. Li, J. R.; Kuppler, R.; Zhou, H., *Chem. Soc. Rev.* **2009,** *38*, 1477.
55. Thomas, K. M., *Catalysis Today* **2007,** *120*, 389-398.

56. Latroche, M.; Surble, S.; Serre, C.; Mellot-Draznieks, C.; Llewellyn, P. L.; Lee, J. H.; Chang, J.-S.; Jhung, S. H.; Ferey, G., *Angew. Chem. Int. Ed* **2006,** *45*, 8227-8231.

57. Schmitz, B.; Muller, U.; Trukhan, N.; Schubert, M.; Ferey, G.; Hirscher, M., *ChemPhysChem* **2008,** *9*, 2181-2184.

Vita

EDUCATION

Master of Science, Chemistry, *Fall 2007- Summer 2010*
Virginia Commonwealth University (VCU), Richmond, Virginia

Chemistry Non-degree, *Fall 2005 –Spring 2007*
Studied Undergraduate and Graduate level chemistry courses
Indiana University – Purdue University Indianapolis (IUPUI), Indianapolis, IN

Bachelor of Education*, 2000-*2002
Utkal University, Regional Institute of Education, Bhubaneswar, Orissa, India

Bachelor of Science, Chemistry (Honors), 1996-1999
University of Burdwan, West Bengal, India
Minor: Physics, Mathematics

PUBLICATION

- Rahimi, Y.; Shrestha, S.; Banerjee, T.; Deo S. K, Reagentless Sensing system for copper based on the far-red fluorescent protein, HcRed from Heteractis crispa, *Analytical Biochemistry*, **2007,** 370, 60-67

POSTER PRESENTATIONS

- Tanushree Banerjee, Ahmed Elzatahry, Karl Jackson, Ahlam Aljarash, Hassan. M. A. Hassan, Victor Abdelsayed, Samy El-Shall, Hani El-Kaderi*,* VCU Departmental Poster Presentation *"Metal Doped Metal-Organic Frameworks for Hydrogen Storage and Catalytic Transformation*" October 10th **2008**

- Tanushree Banerjee, Suresh Shrestha, Yasmeen Rahimi, Sapna K. Deo, IUPUI UROP Summer Poster Symposium *"Expression, Purification and Metal Binding Studies of Dimeric Red Fluorescent Protein, HcRed"* July 21st **2006**

- Tanushree Banerjee, Suresh Shrestha, Yasmeen Rahimi, Sapna K. Deo, IUPUI Undergraduate Research Symposium (UROP) "*Detection of Copper using Monomeric Red Fluorescent Protein"* April 21st **2006**

- Kyle A. Cissel, Tanushree Banerjee, Suresh Shrestha, Ann Goulding, Sapna K. Deo, 6th Annual Indiana Local Section of the American Chemical Society Meeting (Dow Agro Sciences),Indianapolis *"Red Fluorescent Protein in Bioanalysis"* Oct 10th **2005**

AWARD

- IUPUI UROP Research and Learning Award, "Rational Design of Red Fluorescent Protein for Applications in the Development of One-step Assays" Sept **2006**